Environmental Pollution 285 (2021) 117509

Contents lists available at ScienceDirect

Environmental Pollution

journal homepage: www.elsevier.com/locate/envpol

Gamma-irradiation fluctuates the mRNA N^6-methyladenosine (m^6A) spectrum of bone marrow in hematopoietic injury☆

Shuqin Zhang, Jiali Dong, Yuan Li, Huiwen Xiao, Yue Shang, Bin Wang, Zhiyuan Chen, Mengran Zhang, Saijun Fan, Ming Cui *

Tianjin Key Laboratory of Radiation Medicine and Molecular Nuclear Medicine, Institute of Radiation Medicine, Chinese Academy of Medical Sciences and Peking Union Medical College, 238 Baidi Road, 300192, Tianjin, China

ARTICLE INFO

Keywords:
m^6A
MeRIP
Epitranscriptome
Radiation
Hematopoietic injury
Mouse bone marrow

ABSTRACT

Humans benefit from nuclear technologies but consequently experience nuclear disasters or side effects of iatrogenic radiation. Hematopoietic system injury first arises upon radiation exposure. As an intricate new layer of genetic control, the posttranscriptional m^6A modification of RNA has recently come under investigation and has been demonstrated to play pivotal roles in multiple physiological and pathological processes. However, how the m^6A methylome functions in the hematopoietic system after irradiation remains ambiguous. Here, we uncovered the time-varying epitranscriptome-wide m^6A methylome and transcriptome alterations in γ-ray-exposed mouse bone marrow. 4 Gy γ-irradiation rapidly (5 min and 2 h) and severely impaired the mouse hematopoietic system, including spleen and thymus weight, blood components, tissue inflammation and malondialdehyde (MDA) levels. The m^6A content and expression of m^6A related enzymes were altered. Gamma-irradiation triggered dynamic and reversible m^6A modification profiles and altered mRNA expression, where both m^6A fold-enrichment and mRNA expression most followed the (5 min_up/2 h_down) pattern. The CDS enrichment region preferentially upregulated m^6A peaks at 5 min. Moreover, the main GO and KEGG pathways were closely related to metabolism and the classical radiation response. Finally, m^6A modifications correlated with transcriptional regulation of genes in multiple aspects. Blocking the expression of m^6A demethylases *FTO* and *ALKBH5* mitigated radiation hematopoietic toxicity. Together, our findings present the comprehensive landscape of mRNA m^6A methylation in the mouse hematopoietic system in response to γ-irradiation, shedding light on the significance of m^6A modifications in mammalian radiobiology. Regulation of the epitranscriptome may be exploited as a strategy against radiation damage.

1. Introduction

With the development of nuclear-related technology, ionizing radiation has been widely used in industry and medical care. In addition, accidental irradiation exposure may cause severe consequences for living organisms. Iatrogenic irradiation is an effective tool for diagnosis and treatment. For example, radiation therapy curbs tumor growth due to its genotoxicity in the form of DNA damage to cancer cells; however, local normal tissues inevitably suffer from radiotherapeutic side effects. Bone marrow is one of the most sensitive organs to radiation, and hematopoietic system injury arises first when exposed to irradiation rays among the three grades of radiation-induced damage effects (hematopoietic system injury, gastrointestinal system injury and nervous system injury) (Zhang et al., 2019). Generally, DNA breakage to different degrees directly or *via* reactive oxygen species (ROS), further resulting in uncontrollable gene mutations, is regarded as the mechanism underlying radiation toxicity in principle (Nikjoo et al., 2016).

Posttranscriptional modifications of RNA, such as N^1 (or N^6)-methyladenosine (m^1A or m^6A), 7-methylguanine (m^7G) and 5-methylcytosine (m^5C), occur in all domains of life and have been known for longer than 70 years (Amort et al., 2017; Krutyholowa et al., 2019; Ontiveros et al., 2019). Until now, more than 160 different chemical modifications that map to all bases as well as the ribose moiety have been identified in all living organisms (Amort et al., 2017; Chen et al., 2019). Among these modifications, m^6A, deposited at the N^6 position of adenosine by a methyltransferase complex, has been regarded as the

☆ This paper has been recommended for acceptance by Wen Chen.

* Corresponding author.
E-mail address: cuiming0403@bjmu.edu.cn (M. Cui).

https://doi.org/10.1016/j.envpol.2021.117509
Received 20 January 2021; Received in revised form 25 April 2021; Accepted 30 May 2021
Available online 4 June 2021

most pervasive and conservative posttranscriptional modification within eukaryotic messenger RNAs (mRNAs), microRNAs (miRNAs), circular RNAs (circRNAs) and long noncoding RNAs (lncRNAs) (Alarcon et al., 2015; Desrosiers et al., 1974; Patil et al., 2016; Zhang et al., 2020b). The methyltransferase complex consists of three homologous components termed "writers", "erasers" and "readers". The well-known "writer" group catalyzing the formation of m^6A includes methyltransferase-like 3 (METTL3), METTL14, Wilms tumor 1-associated protein (WTAP), KIAA1429 and RNA-binding motif protein 15/15 B (RBM15/15 B) (He et al., 2019). Fat mass and obesity-associated protein (FTO) and alkB homologue 5 (ALKBH5) execute the "eraser" function to selectively remove the methyl group from target RNAs (Frye et al., 2018; He et al., 2019). Recognition of m^6A-modified transcripts is fulfilled by "reader" proteins (such as YT521-B homology (YTH) domain family proteins, IGF2 mRNA binding protein (IGF2BP) families, eukaryotic initiation factor (eIF) 3, and heterogeneous nuclear ribonucleoprotein (HNRNP) protein families), which activate downstream signaling to propel diverse cellular and physiological processes (He et al., 2019; Meyer and Jaffrey, 2017; Muller et al., 2019; Zhao et al., 2017). As a sophisticated control mode of genetic information, a dynamic/reversible profile of m^6A as well as variable expression of effector enzymes is intertwined in various biological processes and governs multiple disease occurrences (Liu and Gregory, 2019; Ma et al., 2018; Roundtree et al., 2017; Zhang et al., 2017), such as solid and hematological cancers (Su et al., 2020), obesity (Zhao et al., 2014), diabetes mellitus (Yang et al., 2020), infertility (Hu et al., 2020; Song et al., 2020), neuronal disorder (Yoon et al., 2017), infectious diseases (Hao et al., 2019), developmental delay (Li et al., 2018) and facial dysmorphism (Richard et al., 2019).

Homeostasis imbalance and external environmental stimuli elicit variable posttranscriptional modifications. For instance, abnormal epitranscriptomic signatures are observed in multiple diseases, such as hypertension (Zhang et al., 2018), insulin resistance (De Jesus and Kulkarni, 2019) and stress-related psychiatric disorders (Engel et al., 2018); ultraviolet rays (Xiang et al., 2017), photobiological alterations (Robinson et al., 2019), circadian clock (Zhong et al., 2018), hypoxia/reoxygenation (Song et al., 2019) and heat stress (Lu et al., 2019) fluctuate dynamic m^6A RNA methylation in sophisticated manners. Although the relationship between m^6A modification and the radiobiology of cancers has been most reported (Chi et al., 2018; Guo et al., 2020; Taketo et al., 2018; Visvanathan et al., 2018), the epitranscriptome-wide m^6A profile present in the hematopoietic system after irradiation challenge has not been illustrated.

Thus, we aimed to acquire a detailed inspection of m^6A methylation in poly(A)-RNAs in the mouse hematopoietic system after γ-irradiation exposure. To this end, we performed global methylated (m^6A) RNA immunoprecipitation with high-throughput sequencing (MeRIP-seq) for mouse bone marrow after 4 Gy γ-irradiation and analyzed the evolving patterns of the m^6A methylome of mRNA at 0 min, 5 min and 2 h postirradiation. Additionally, the transcriptome alterations responding to irradiation treatment were also presented, accompanied by correlation analyses of posttranscriptional m^6A methylation and transcriptional gene expression. Finally, we preliminarily explored the effect of γ-irradiation on the radiosensitivity of mice after certain m^6A modulating enzymes were blocked *in vivo*. Collectively, our findings provide the comprehensive landscape of mRNA m^6A methylation as well as transcriptome regulation in the mouse hematopoietic system following γ-irradiation, shedding light on the significance of the m^6A modification in the mammalian response to radiation in mammals.

2. Materials and methods

2.1. Statistical analysis

The data were analyzed using the appropriate statistical analysis methods and presented as the means ± SEMs with respect to the number of samples (n) in each group. Student's *t*-test was used to analyze the statistical significance between two independent groups. For categorical variables, Fisher's exact test was used. For enrichment analysis, *P* values were adjusted using the Benjamini-Hochberg algorithm as indicated in the figure legends, and P values < 0.05 were considered statistically significant.

2.2. Data availability

The data that support the findings of this study are available from the corresponding author upon reasonable request.

3. Results

3.1. Gamma-irradiation triggers hematopoietic system injury accompanied by alterations of m^6A modification levels and the expression of m^6A modulating enzymes

The hematopoietic organs from C57BL/6 J mice, such as the spleen and thymus, were atrophied in a short time (5 min and 2 h) after 4 Gy γ-irradiation exposure (Fig. 1A and B). Multiple hematological parameters, including white blood cells (WBCs), lymphocytes and platelets (PLTs), also severely changed within 2 h (Fig. 1C–K). Additionally, interleukin 6 (IL-6), tumor necrosis factor-α (TNF-α) and the lipid peroxidation product malondialdehyde (MDA) were increased after radiation stimuli, suggesting that irradiation rapidly elevates the inflammatory status and oxidative stress (Fig. 1L–N). To outline the alterations in the hematopoietic m^6A methylome following irradiation at an early stage, we collected bone marrow cells at 0 min, 5 min and 2 h from C57BL/6 J mice after 4 Gy radiation exposure to detect the difference of global m^6A content. LC-MS/MS assay showed that the m^6A modification level in irradiated bone marrow cells reduced at 2 h, while there was a slight elevation at 5 min (Fig. 1O). We further measured the expression of five pivotal m^6A effector enzymes (3 "writers" *METTL3*, *METTL14* and *WTAP*, 2 "erasers" *FTO* and *ALKBH5*) at the three time points. Interestingly, the mRNA of these enzymes exhibited distinct expression profiles. In detail, the expression of *METTL3*, *WTAP* and *FTO* down-regulated while those of *METTL14* and *ALKBH5* up-regulated both at 5 min and 2 h. Compared with 5 min, the expression levels of *METTL3* and *ALKBH5* at 2 h up-regulated while *WTAP* down-regulated (Fig. 1P–T). Consistently, the protein expression levels of the enzymes confirmed the tendency (Fig. 1U). Combining the results of m^6A content and expression of levels of related enzymes, irradiation may regulate the hematopoietic m^6A methylome profile, "writers" METTL14 (WTAP) and "erasers" FTO (ALKBH5) at 5 min (2 h) may play major roles in the development of radiation toxicity of bone marrow cells after total body irradiation (TBI).

3.2. The time-dependent m^6A methylation spectrum of mRNA in the bone marrow of irradiated mice

Given that bone marrow is most sensitive hematopoietic organ and hematopoietic inhibition of bone marrow is a major reason for radiation accidental death or adverse reactions of radiotherapy (Dainiak and Sorba, 1997; Zhang et al., 2013), we collected the bone marrow cells of mice sacrificed at 0 min, 5 min and 2 h post γ-irradiation and extracted the total RNA for MeRIP-seq analysis. As shown in Fig. 2A, a Venn diagram showed that there was a total of 544, 211 and 210 calling mRNA peaks of the Ctrl, 5 min and 2 h groups, respectively (analyzed according to the common peaks of every three replicates in each group, Data S1). Among them, the time-specific peaks outnumbered the common peaks shared by two or three time points (except the 5 min/Ctrl comparison), and only 51 peaks existed in all three groups. Moreover, the specific peaks of the 5 min or 2 h group were far fewer than those of the Ctrl group, whereas there was approximately the same number between the 5 min and 2 h groups. The data suggest that 4 Gy γ-irradiation causes a

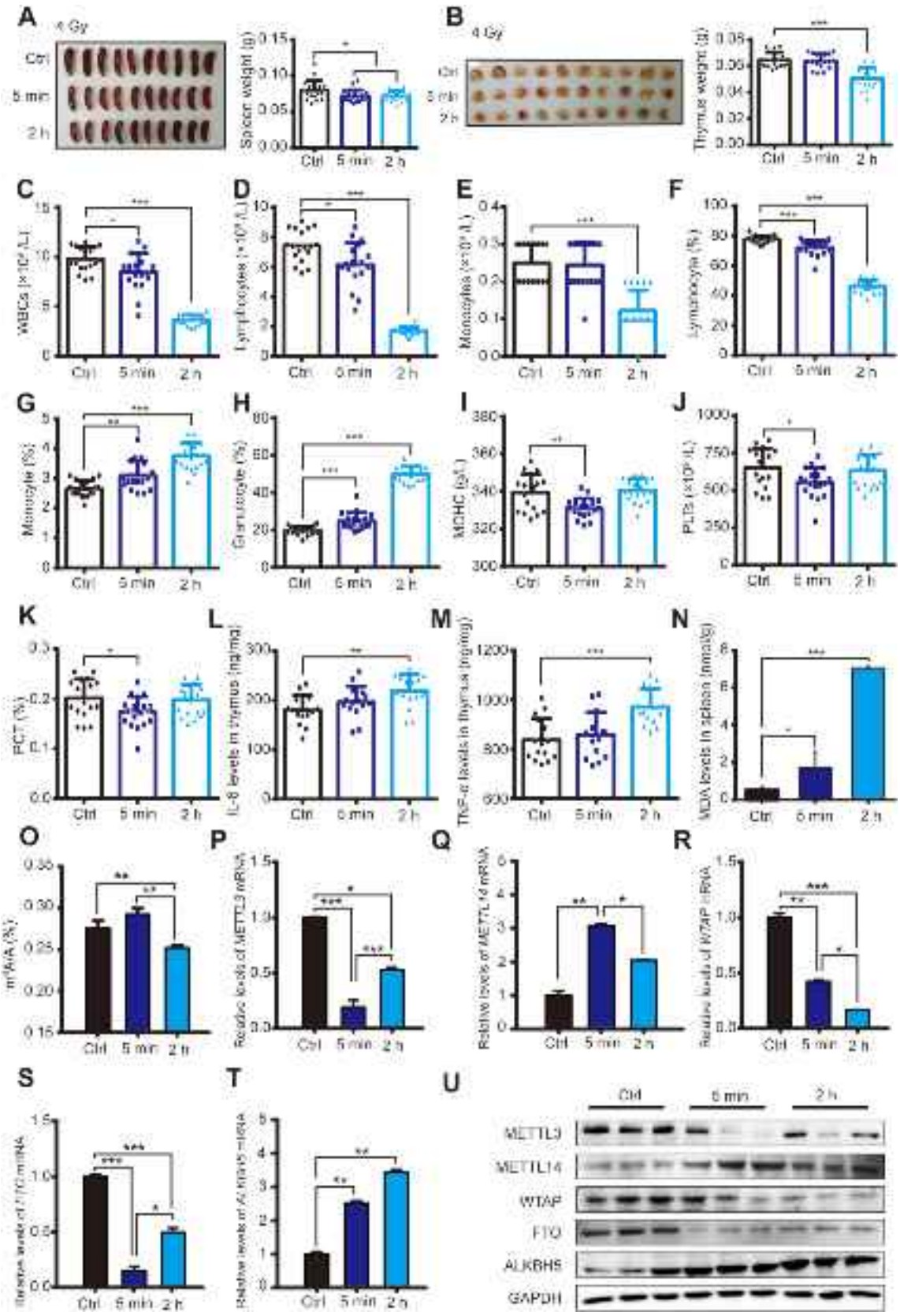

(caption on next page)

Fig. 1. Gamma-irradiation triggers hematopoietic system injury accompanied by alterations of m^{6}A modification levels and the expression of m^{6}A modulating enzymes. (A, B) Images and weights of the spleen (A) and thymus (B) of C57BL/6 J mice at 0 min, 5 min and 2 h after exposure to 4 Gy γ-irradiation. (n = 18). (C–K) Blood from C57BL/6 J mice was collected from the orbital sinus at 0 min, 5 min and 2 h after exposure to 4 Gy γ-irradiation. The blood parameters were analyzed using a Celltac E hemocytometer (Nihon Kohden, Japan), and the levels of white blood cells (WBCs) (C), lymphocytes (D), monocytes (E), lymphocyte (%) (F), monocyte (%) (G), granulocyte (%) (H), mean corpuscular hemoglobin concentration (MCHC) (I), platelets (PLT) (J) and plateletcrit% (PCT%) (K) after irradiation are shown. (n = 18). (L, M) Levels of the proinflammatory cytokines IL-6 and TNF-α in thymus tissues at different time points were detected by ELISA. (N) The MDA content within spleen tissues at different time points was measured with a specific MDA detection kit. (n = 18). (O) The variation of global m^{6}A modification levels at 0 min, 5 min and 2 h after γ-ray exposure was determined by LC-MS/MS analysis. (n = 3, 1 replicate consisted of a mixture of bone marrow cells from every four mice in one group). (P–T) The mRNA expression levels of five m^{6}A modification related enzymes *METTL3* (P), *METTL14* (Q), *WTAP* (R), *FTO* (S) and ALKBH5 (T) in mouse bone marrow at 0 min, 5 min and 2 h after γ-ray exposure were monitored by qRT-PCR. (n = 12). (U) The protein expression levels of five m^{6}A modification related enzymes *METTL3* (P), *METTL14* (Q), *WTAP* (R), *FTO* (S) and ALKBH5 (T) in mouse bone marrow at 0 min, 5 min and 2 h after γ-ray exposure were measured by Western blot. (n = 3, 1 replicate consisted of a mixture of bone marrow cells from every four mice in one group). Data are shown as the mean ± SEM of three independent experiments. Statistically significant differences are indicated: *, $P < 0.05$; **, $P < 0.01$; ***, $P < 0.001$; Student's *t*-test.

rapid and time-dependent m^{6}A mRNA signature. Moreover, mapping of the methylated positions to the reference genome revealed that the m^{6}A modifications were located in 378 (Ctrl), 223 (5 min) and 178 (2 h) annotated genes, respectively. The relative numbers of common or specific genes in the three groups were similar to the m^{6}A features (Fig. 2B, Data S2). On average, genes in the Ctrl, 5 min or 2 h group harbored 1.439 (544/378), 0.946 (211/223) or 1.180 (210/178) m^{6}A modifications, respectively, exhibiting a "down then up" trend that was similar to certain m^{6}A enzyme trends. These results indicate that 4 Gy γ-irradiation induces a reduction in both m^{6}A sites and m^{6}A-modified transcripts in a short time. Then, we analyzed the differential expression profile of transcripts between each pair of time points and found that most of the differential transcripts were shared by two or three comparisons, implying that the majority of the transcripts change their expression pattern over time after radiation challenge (Fig. 2C, Data S3). Notably, most transcripts in each replicate carried only one peak, among which the m^{6}A-modified transcripts increased at 5 min but decreased at 2 h (Fig. 2D, Data S4). Five minutes after irradiation, the m^{6}A peaks with a lower enrichment fold (<10) decreased whereas the peaks with a higher enrichment fold (>10) increased. However, all m^{6}A peaks at 2 h exhibited the opposite patterns (Fig. 2E, Data S5). The relationship between the score and number of m^{6}A modifications in each replicate was also shown (Fig. S1A, Data S6).

Additionally, most of the m^{6}A sites corresponded to the annotated transcripts, and the proportion of these transcripts was elevated 5 min after irradiation. Intriguingly, m^{6}A peaks in the 5′UTR were less changeable within 2 h, however, the peaks mapped to the CDS and 3′UTR regions experienced an increase (5 min) and then reverse (2 h) trend (Fig. 2F, Data S7). As shown in Fig. 2G and Fig. S1B-D, m^{6}A summits in the CDS, stop codon and 3′UTR remained the dominant position in all sites, which was consistent with previous reports (Dominissini et al., 2012; Jabs et al., 2020). In addition, m^{6}A peaks in the Ctrl and 2 h groups had a higher MeRIP enrichment in the 5′UTR and stop codon regions, but the 5 min group harbored relatively higher enrichment of m^{6}A peaks in the CDS and stop codon regions. Specifically, m^{6}A enrichment in the transcriptional start site (TSS) and 5′UTR exhibited a "down then up" tendency, while that in the CDS showed the opposite pattern (Fig. 2H). In addition, the number of common or summational MeRIP peaks of each three replicates both showed an "up and down" trend for the enrichment pattern in the CDS and 3′UTR regions, whereas those in intronic regions presented reverse alterations (Fig. 2I, Fig. S1E). Then, we conducted motif searches for all detected peaks and assessed the prevalence of the motifs in the three groups. Similar to the known RRACH (R = A or G, H = A, C or U) sequence (Dominissini et al., 2012; Jabs et al., 2020), most detected motifs exhibited a gradual decrease at 5 min and 2 h after irradiation (Fig. 2J, Data S8). Specifically, there were also certain peaks of distinct genes displaying the "change then recover" or conserved m^{6}A style, such as the peaks at the indicated sites of *Tfdp1* ("up then down"), *Elk4* ("down then up") and *Rnf19a* (conserved) (Fig. 2K-M, left panel). MeRIP-qPCR was performed to further confirm the phenomena (Fig. 2K-M, right panel).

Collectively, the results indicate that (1) a temporal variable m^{6}A signature of mRNA is implicated in the response of bone marrow to 4 Gy γ-irradiation, (2) the overall m^{6}A spectrum at 5 min following irradiation is upregulated and then downregulated at 2 h, and (3) the mRNA m^{6}A landscape, including the frequency, enrichment extent and distribution pattern, presents an "alter then recover" tendency in the short-term evolving process following irradiation.

3.3. Differentially methylated m^{6}A peaks between different time points

Next, we analyzed the detailed methylated m^{6}A peaks between each set of time points according to reads per million (RPM) values and identified 3774 (1709 up/2065 down), 3906 (2097 up/1809 down) and 3703 (1789 up/1914 down) differential peaks in the comparison of (5 min vs Ctrl), (2 h vs 5 min) and (2 h vs Ctrl), respectively (Fig. 3A–C, Data S9 and S10). Concretely, m^{6}A peaks that were upregulated in the 5 min group harbored more peaks in the CDS region but fewer peaks in the 5′UTR region than those that were downregulated (Fig. 3D, Data S11). This characteristic was verified from the peak accumulation curve plot (Fig. 3E–G). The above m^{6}A peaks in IP samples were also analyzed in the corresponding Input samples to investigate the correlation between mRNA expression and m^{6}A peaks (Fig. S2A-C, Data S12).

3.4. The signature of m^{6}A peaks exhibits different evolving trends after γ-irradiation stimulation

Then, we further investigated the time-dependent m^{6}A methylation profile and identified 4 classes of m^{6}A peaks with distinct evolving types (5 min_up/2 h_up, 5 min_down/2 h_down, 5 min_up/2 h_down and 5 min_down/2 h_up) according to the fold enrichment. The data showed that there were 56, 26, 1215, and 1029 peaks in the clusters, respectively (Fig. 4A–D, Data S13). As shown in the heatmaps, the numbers of m^{6}A peaks in the (5 min_up/2 h_down) and (5 min_down/2 h_up) groups overwhelmed those in the other two continuously changing groups, especially in the (5 min_up/2 h_down) group (possessing 52.24% of all the peaks of the four groups). The best-fit curves of the m^{6}A peaks further confirmed the results (Fig. 4E–H). Regarding the distribution features, substantial m^{6}A peaks in the (5 min_up/2 h_down) group were concentrated in the CDS and 3′UTR regions, whereas those in the (5 min_down/2 h_up) group were distributed in a relatively average distribution. No meaningful pattern could be found for m^{6}A peaks in the other two groups due to the limited quantity (Fig. 4I). Moreover, the representative m^{6}A sites on certain genes in each cluster (*Tra2a* in "5 min_up/2 h_up", *Jak1* in "5 min_down/2 h_down", *Jun* in "5 min_up/2 h_down" and *Rbm12(Cpne1)* in "5 min_down/2 h_up") were shown by IGV software (Fig. 4J-M, left panel), and MeRIP-qPCR assay further verified the variational pattern of these peaks (Fig. 4J-M, right panel).

3.5. mRNAs with differential m^{6}A evolving patterns are implicated in general, specific or opposite biological pathways

To further explore whether m^{6}A methylation relates to irradiation response and injury repair signaling, mRNAs of the four categories were

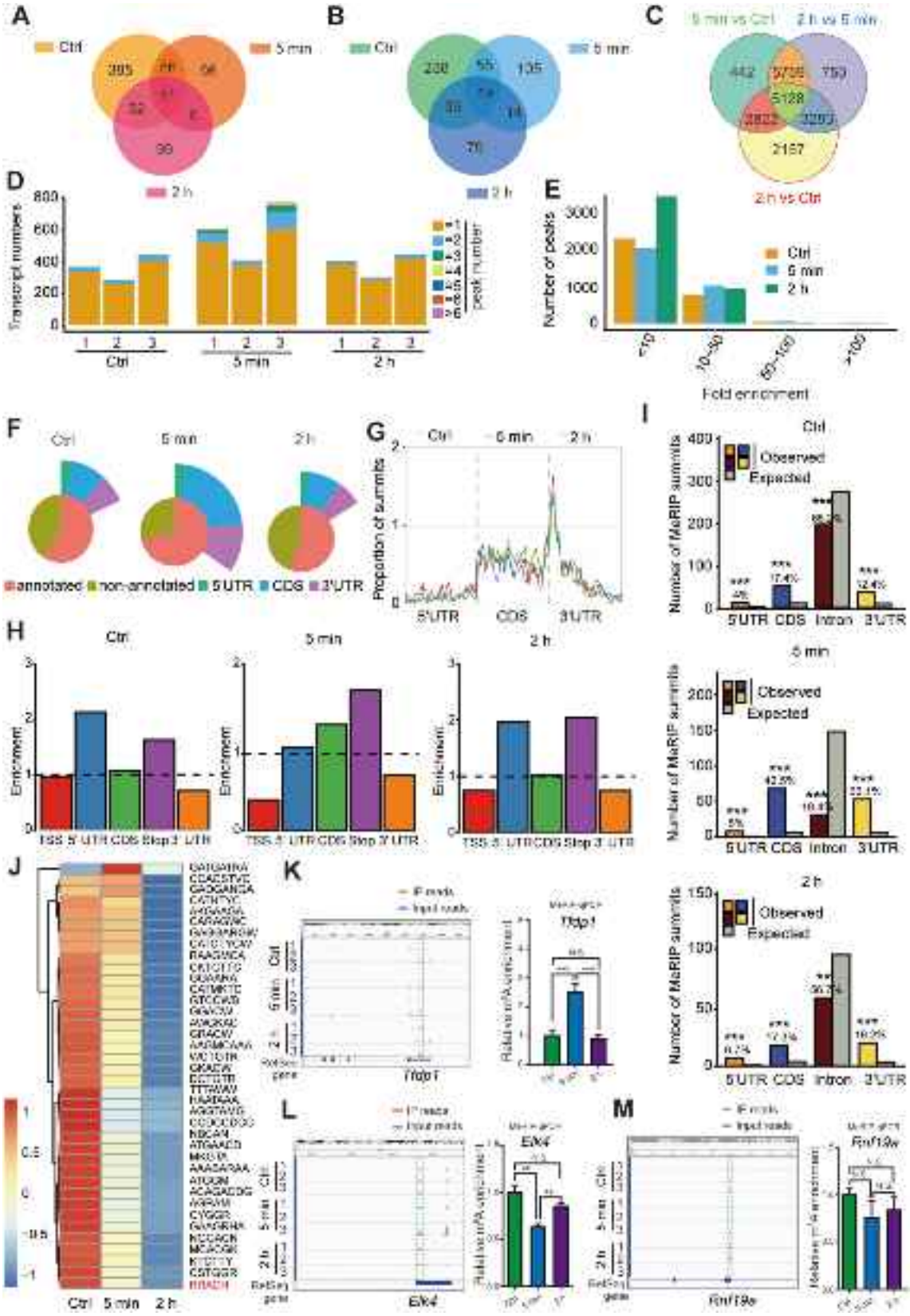

(caption on next page)

Fig. 2. The time-dependent m^{6}A methylation spectrum of mRNA in the bone marrow of irradiated mice. (A) Venn diagram of the common m^{6}A peaks of every three replicates at 0 min, 5 min and 2 h after γ-irradiation of 4 Gy. (B) Venn diagram representing the number of genes to which the identified m^{6}As were mapped. (C) Venn diagram of differentially expressed transcripts in each comparison of 5 min vs Ctrl (or 2 h vs 5 min, or 2 h vs Ctrl). (D) Counts of transcripts harboring different numbers of m^{6}A peaks in each sample of mouse bone marrow from the Ctrl, 5 min and 2 h groups. (E) Number of m^{6}A peaks with different fold enrichment in each group of Ctrl, 5 min and 2 h. (F) The distribution ratios of m^{6}A sites in annotated/unannotated transcripts or across different mRNA regions of the 5′UTR, CDS and 3′UTR at each time point are shown in a two-level pie chart. (G) Curves of best fit visually displaying the accumulation patterns of m^{6}A peaks along the full-length mRNA transcripts in the Ctrl, 5 min and 2 h groups. Each transcript was divided into three parts: 5′UTR, CDS and 3′UTR. (H) The enrichment degree of m^{6}A peaks dispersed in each segment (TSS, 5′UTR, CDS, stop codon and 3′UTR) of the mRNAs in each group. (I) The number and relative proportions of MeRIP peaks dispersed in different sections (5′UTR, CDS, intron and 3′UTR) of the mRNAs in each group. The number or proportion are for the common peaks of every three samples in each group. The expected number (gray colored) of each section in the condition of even alignment is also shown. Fisher's exact test, **, $P \leq 0.005$. (J) Heatmap showing the m^{6}A motif enrichment determined by calculating the occurrence ("high" in red and "low" in blue) of motifs in total m^{6}A peaks in the Ctrl, 5 min and 2 h groups. The consensus motif of RRACH is highlighted in red. (K–M) Representative genes bearing m^{6}A peaks with the "up then down" (K, *Tfdp1*), "down then up" (L, *Elk4*) or conserved (M, *Rnf19a*) tendencies among the three groups are exhibited by IGV software. "IP" in red and "Input" in blue. The variation trends of the indicated peaks were verified by MeRIP-qPCR analyses (right panels). Statistically significant differences are indicated: **, $P < 0.01$; ***, $P < 0.001$; Student's *t*-test. N.S., no significance. (For interpretation of the references to color in this figure legend, the reader is referred to the Web version of this article.)

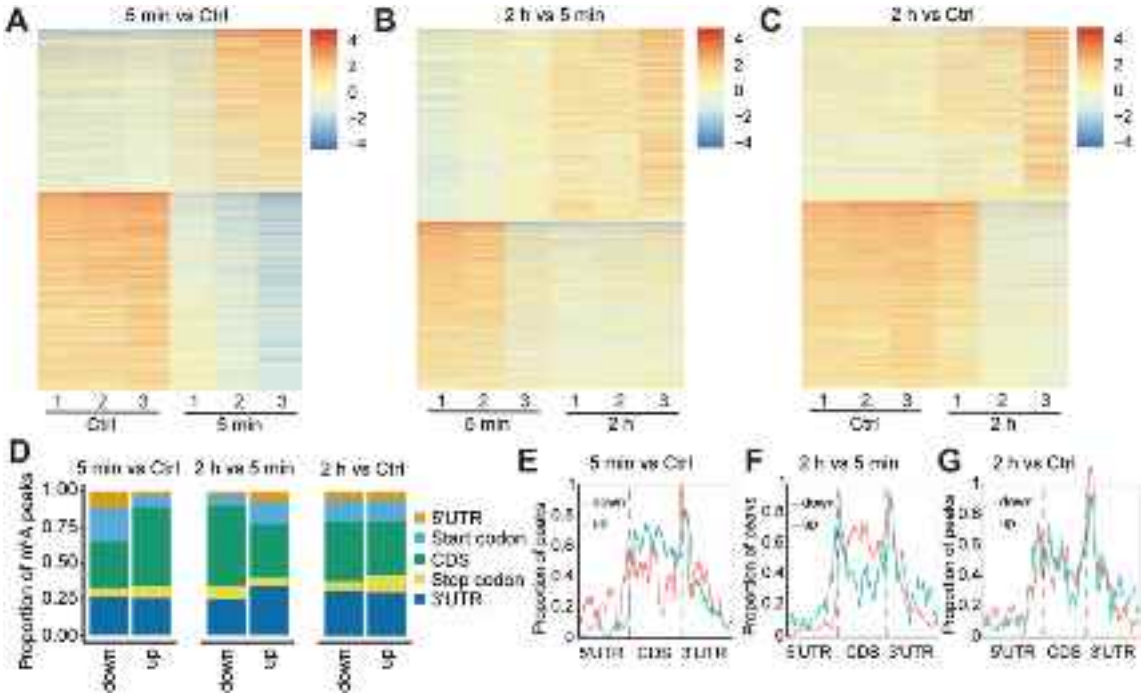

Fig. 3. Differentially methylated m^{6}A peaks between different time points. (A–C) Heatmaps presenting the differentially ("up" in red and "down" in blue) methylated m^{6}A peaks in the comparison of 5 min vs Ctrl (A), 2 h vs 5 min (B), or 2 h vs Ctrl (C). The upper panel shows the peaks that were upregulated, while the lower panel shows the peaks that were downregulated. Log_2 fold change >1 or < -1 is regarded as the threshold of the region defined as differential methylation region. (D) Stacked bar plot showing the percentage of down/up-methylated m^{6}A peaks corresponding to each segment (5′UTR, start codon, CDS, stop codon and 3′UTR) of mRNA in the comparison of 5 min vs Ctrl (or 2 h vs 5 min, or 2 h vs Ctrl). (E–G) Curves of best fit visually displaying the accumulation features of down/upregulated m^{6}A peaks in the comparison of 5 min vs Ctrl (E), 2 h vs 5 min (F), or 2 h vs Ctrl (G), along the full-length mRNA transcript. Each transcript was divided into three parts: 5′UTR, CDS and 3′UTR. (For interpretation of the references to color in this figure legend, the reader is referred to the Web version of this article.)

subjected to Gene Ontology (GO) enrichment and Kyoto Encyclopedia of Genes and Genomes (KEGG) pathway analyses. We mainly focused on those with the (5 min_up/2 h_down) and (5 min_down/2 h_up) trends (Fig. 5A–D, Data S14), for the gene numbers in other two groups were less than 10 (Fig S3A-D, Data S15). For the biological process (BP) category, although metabolism-related terms were commonly shared by the (5 min_up/2 h_down) and (5 min_down/2 h_up) groups, certain other GO terms were oppositely enriched in the two groups; for instance, the terms regulation of biological process, cellular process, metabolic process, and macromolecule metabolic process. Several other terms were group-specific, such as organic substance metabolic process and regulation of protein metabolic regulation of protein metabolic processes, cell death as well as apoptotic processes in the (5 min_up/2 h_down) group; cellular nitrogen compound biosynthetic process, gene expression, RNA biosynthetic process and biosynthetic process in the (5 min_down/2 h_up) group. Irradiation is a typical stress stimulus in organisms (Mishra and Luderer, 2019), and GO enrichment analysis also identified m^{6}A methylated transcripts linked to response to stress and regulation of response to stress in the (5 min_up/2 h_down) group.

For the cellular component (CC) category, the enrichment terms of the (5 min_up/2 h_down) cluster were mainly concentrated in the extracellular regions, while those of the (5 min_down/2 h_up) cluster were mainly concentrated in the intracellular part or intracellular organelle (Fig. 5A and B). With respect to molecular function (MF), items dominating in the (5 min_up/2 h_down) cluster were mainly binding and protein binding, whereas molecules functioning in binding to carbohydrate derivatives, chromatin and adenyl nucleotides exhibited a relatively pervasive position in the (5 min_down/2 h_up) cluster, hinting at distinct biological features of m^{6}A-methylated mRNAs with the opposite fluctuating tendency (Fig. 5A and B).

Regarding the KEGG pathway, the two clusters shared certain pathway terms, including spliceosome, ribosome, PI3K-AKT signaling

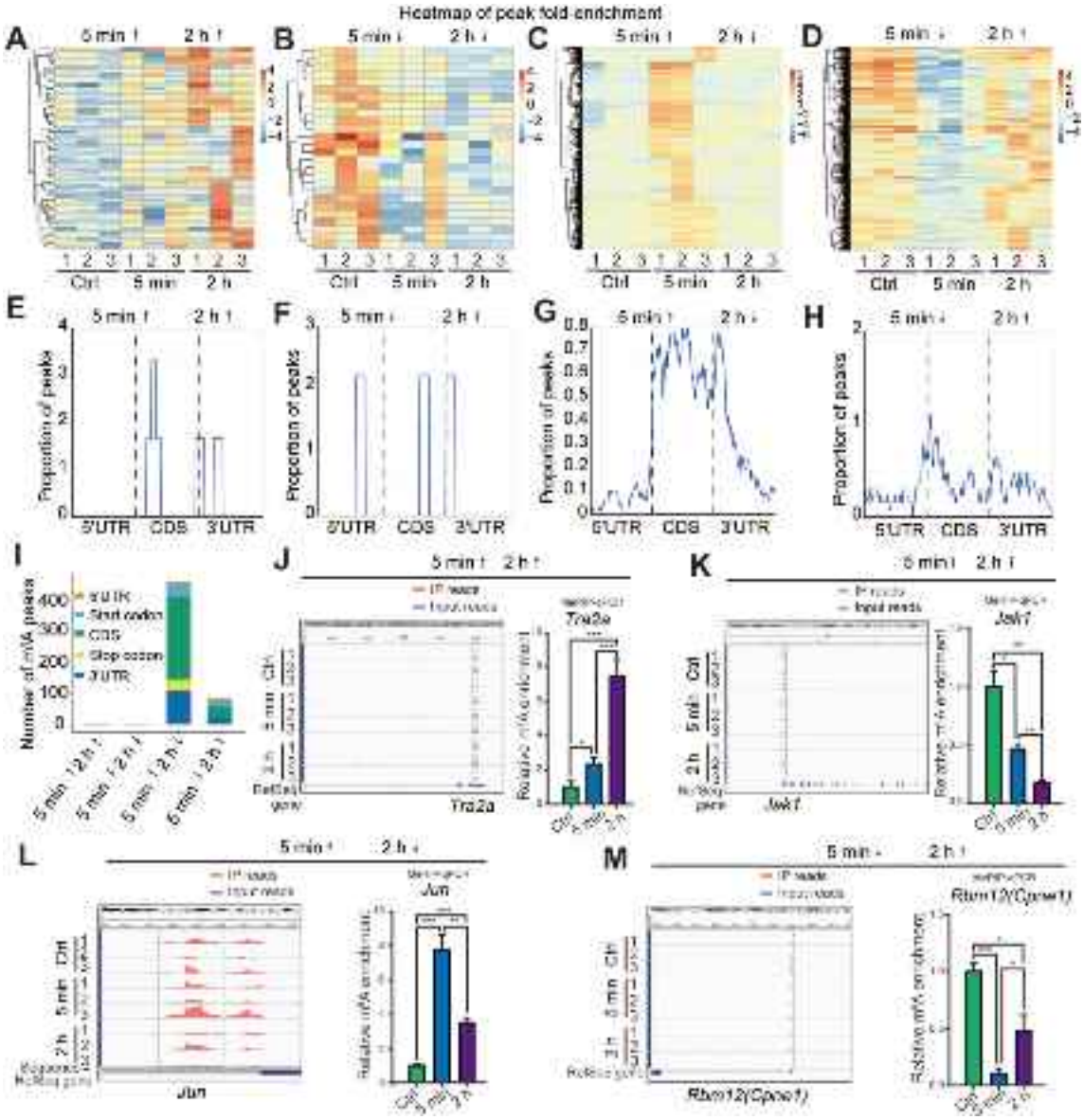

Fig. 4. The signature of m^{6}A peaks exhibits different evolving trends after γ-irradiation stimulation. (A–D) Heatmaps representing the differentially ("up" in red and "down" in blue) methylated m^{6}A peaks with evolving patterns of (5 min_up/2 h_up) (A), (5 min_down/2 h_down) (B), (5 min_up/2 h_down) (C) and (5 min_down/2 h_up) (D) among the three Ctrl, 5 min and 2 h groups. The peaks of 9 samples in 3 groups were merged, followed by the RPM and fold enrichment computation for each sample to acquire the differential (up and down) methylational peaks in (5 min_vs_Ctrl) and (2 h_vs_5 min) comparisons, eventually, taking the intersection between each (5 min_vs_Ctrl)_up/down and each (2 h_vs_5 min) _up/down cluster obtained the corresponding four tendencies. (E–H) The respective accumulation profiles of differentially methylated m^{6}A peaks with the regulatory patterns of (5 min_up/2 h_up) (E), (5 min_down/2 h_down) (F), (5 min_up/2 h_down) (G) and (5 min_down/2 h_up) (H) along the transcripts. Each transcript was divided into three segments: 5′UTR, CDS and 3′UTR. (I) Stacked bar plot displaying the distribution characteristics of m^{6}A peaks in different regions (5′UTR, start codon, CDS, stop codon and 3′UTR) of normalized mRNAs. (J–M) Representative m^{6}A peaks with different evolving patterns on certain genes (5 min_up/2 h_up peaks on *Tra2a*, J), (5 min_down/2 h_down peaks on *Jak1*, K), (5 min_up/2 h_down peaks on *Jun*, L) and (5 min_down/2 h_up peaks on *Rbm12 (Cpne1)*, M) are exhibited by IGV software. "IP" in red and "Input" in blue. The variation trends of the indicated peaks were verified by MeRIP-qPCR analyses (right panels). Statistically significant differences are indicated: *, $P < 0.05$; **, $P < 0.01$; ***, $P < 0.001$; Student's *t*-test. (For interpretation of the references to color in this figure legend, the reader is referred to the Web version of this article.)

pathway, metabolic pathways and Alzheimer's disease. In addition, pathways involving steroid hormone biosynthesis, retinol metabolism and inflammatory mediator regulation of TRP channels were particularly enriched in the (5 min_up/2 h_down) group, while pathways of RNA transport, p53 signaling pathway and leukocyte transendothelial migration specifically enriched in the (5 min_down/2 h_up) group (Fig. 5C and D). Of note, pathways of oxidative phosphorylation, hypoxia-inducible factor 1 (HIF-1) and oxytocin signaling were also identified in KEGG analysis of the clusters (Fig. 5C and D), which was in accordance with the common knowledge that irradiation produces substantial free superoxide radicals and causes oxidation-associated reactions in tissues (Anastassopoulou and Theophanides, 2002; Zhang and Martin, 2014).

3.6. Time-variably expressed mRNAs participate in diverse biological pathways

Then, we performed transcriptomic analyses for bone marrow mRNAs at 0 min, 5 min and 2 h after 4 Gy γ-irradiation. As shown in Fig. 6A and B, the differential mRNAs were categorized into two classes,

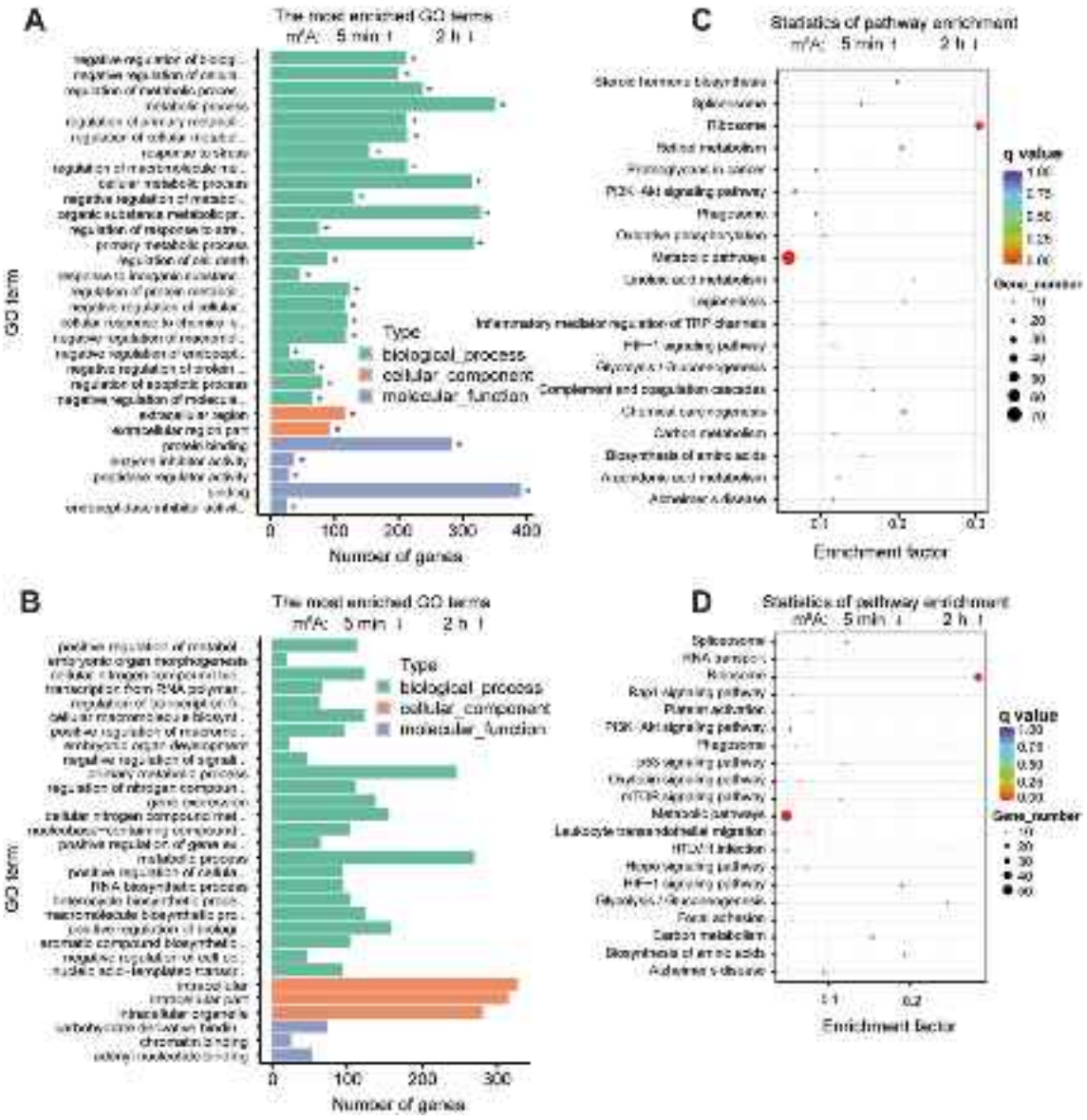

Fig. 5. mRNAs with differential m^{6}A evolving patterns are implicated in general, specific or opposite biological pathways. (A) The most enriched GO terms, including biological process, cellular component and molecular function, for m^{6}A methylation with the evolving pattern of (5 min_up/2 h_down). (B) The most enriched GO terms, including biological process, cellular component and molecular function, for m^{6}A methylation with the evolving pattern of (5 min_down/2 h_up). (C) The statistics of enriched pathways for differential m^{6}A sites with the pattern of (5 min_up/2 h_down). (D) The statistics of enriched pathways for differential m^{6}A sites with the pattern of (5 min_down/2 h_up). The *P* value of enrichment statistical analyses was corrected by the Benjamini-Hochberg algorithm, also called q value, *, $P < 0.05$.

including 3 subtypes for each class, based on the shift paradigm. The results showed that the greater the fold change was, the more enriched genes presented in all subtypes. For the "Up" class, the ratio of genes in the >5 fold change subtype experienced a "first down then up" trend over time, while that in the 2 < 5 fold change subtype displayed the inverse paradigm (Fig. 6A, Data S16). In the "Down" class, the ratio of genes in the fold change <1/5 (or fold change > 1/2) subtype decreased (or increased) over time (Fig. 6B, Data S17). Then, we depicted the heatmaps of differentially expressed mRNAs with the evolving patterns of (5 min_up/2 h_up), (5 min_down/2 h_down), (5 min_up/2 h_down) and (5 min_down/2 h_up) and identified 676, 329, 5742 and 4140 mRNAs in each category, respectively (Fig. 6C–F, Data S18). The relative distribution of mRNA numbers among the four groups was roughly consistent with that of m^{6}A peaks. GO enrichment and KEGG pathway analyses were also performed for mRNAs with the above tendencies. Consistent with m^{6}A methylation, metabolism-related processes were most enriched in both groups according to the BP analyses. Nevertheless, other items containing localization, macromolecule modification and protein modification processes were uniquely owned by the (5 min_up/2 h_down) group, and items including nitrogen compound metabolic process, nucleobase-containing compound and cellular aromatic compound metabolic process were specifically possessed by the (5 min_down/2 h_up) group. For the CC analyses, terms such as intracellular part, cytoplasm, organelle and membrane-bounded organelle were shared by both groups, whereas items of cell part and cell which took the dominant position uniquely existed in the (5 min_up/2 h_down) group and some nuclear components such as nucleus, nuclear part and nuclear lumen plus several lumen-related components were particularly affiliated with the (5 min_down/2 h_up) group. Furthermore, categories related to binding function such as ion, cation and protein binding, as well as catalytic activity, were identified in the MF analyses of the (5 min_up/2 h_down) group, while no obvious MF enrichment was found in

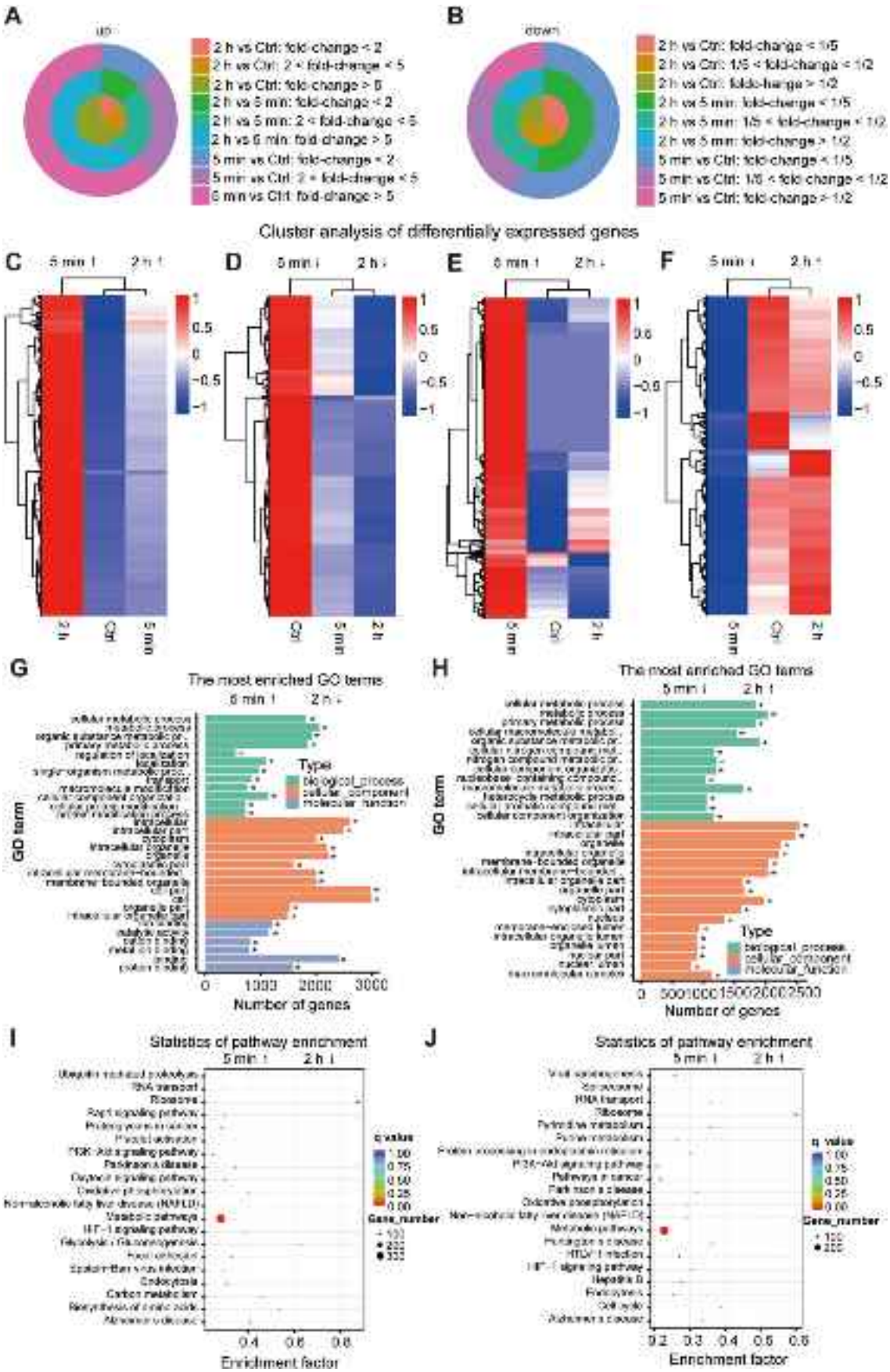

(caption on next page)

Fig. 6. Time-variably expressed mRNAs participate in diverse biological pathways. (A) The pie chart showing the fold distribution of upregulated genes in the comparison of 2 h vs Ctrl (or 2 h vs 5 min, or 5 min vs Ctrl). (B) The pie chart showing the fold distribution of downregulated genes in the comparison of 2 h vs Ctrl (or 2 h vs 5 min, or 5 min vs Ctrl). (C–F) Cluster analysis for differentially ("up" in red and "down" in blue) expressed genes with the tendencies of (5 min_up/2 h_up) (C), (5 min_down/2 h_down) (D), (5 min_up/2 h_down) (E) and (5 min_down/2 h_up) (F) among the three groups. (G, H) The most enriched GO terms, including biological process, cellular component and molecular function, for genes with expression trends of (5 min_up/2 h_down) (G) and (5 min_down/2 h_up) (H). (I, J) The statistics of respective enriched pathways for differentially expressed genes with the trends of (5 min_up/2 h_down) (I) and (5 min_down/2 h_up) (J). The *P* value of statistical analysis for enrichment was corrected by the Benjamini-Hochberg algorithm, also called q value, *, $P < 0.05$. (For interpretation of the references to color in this figure legend, the reader is referred to the Web version of this article.)

the (5 min_down/2 h_up) group (Fig. 6G and H, Data S19).

Approximately half of the KEGG pathways were distinct between the (5 min_up/2 h_down) and (5 min_down/2 h_up) groups except certain common terms such as RNA transport, ribosome, oxidative phosphorylation and Alzheimer's disease. Pathways covering glycolysis/gluconeogenesis, biosynthesis of amino acids, carbon metabolism and ubiquitin-mediated proteolysis were most preferably enriched in the cluster of the (5 min_up/2 h_down) group, and pathways including cell cycle, Huntington's disease and pyrimidine metabolism were most preferably enriched in the (5 min_down/2 h_up) group. Notably, the pathway of platelet activation associated with irradiation-induced hematopoiesis was among the cluster of the (5 min_up/2 h_down) group (Fig. 6I and J, Data S20). In addition, GO enrichment and KEGG pathway analyses for the (5 min_up/2 h_up) and (5 min_down/2 h_down) groups were conducted, and the results are presented in Figure S4A-D, but substantially fewer genes were identified in the two classes.

3.7. Correlation analyses between mRNA m^{6}A methylation and gene expression

Then, we investigated the relationship between m^{6}A methylation and the gene expression of mRNAs. As shown in Fig. 7A–C, genes with higher expression levels contained higher proportions of m^{6}A modification, and the ratios of methylated mRNAs increased after irradiation (both at 5 min and 2 h) when the expression deciles ≥ 6, among which genes with deciles of 9 and 10 had "increase then fall" rates over time. Regarding the expression of genes with temporally specific m^{6}A peaks, no distribution preference could be found between each pair of time points, implying that irradiation influences mRNA m^{6}A methylation indispensable of time-variable gene activation, and mRNA epigenetic

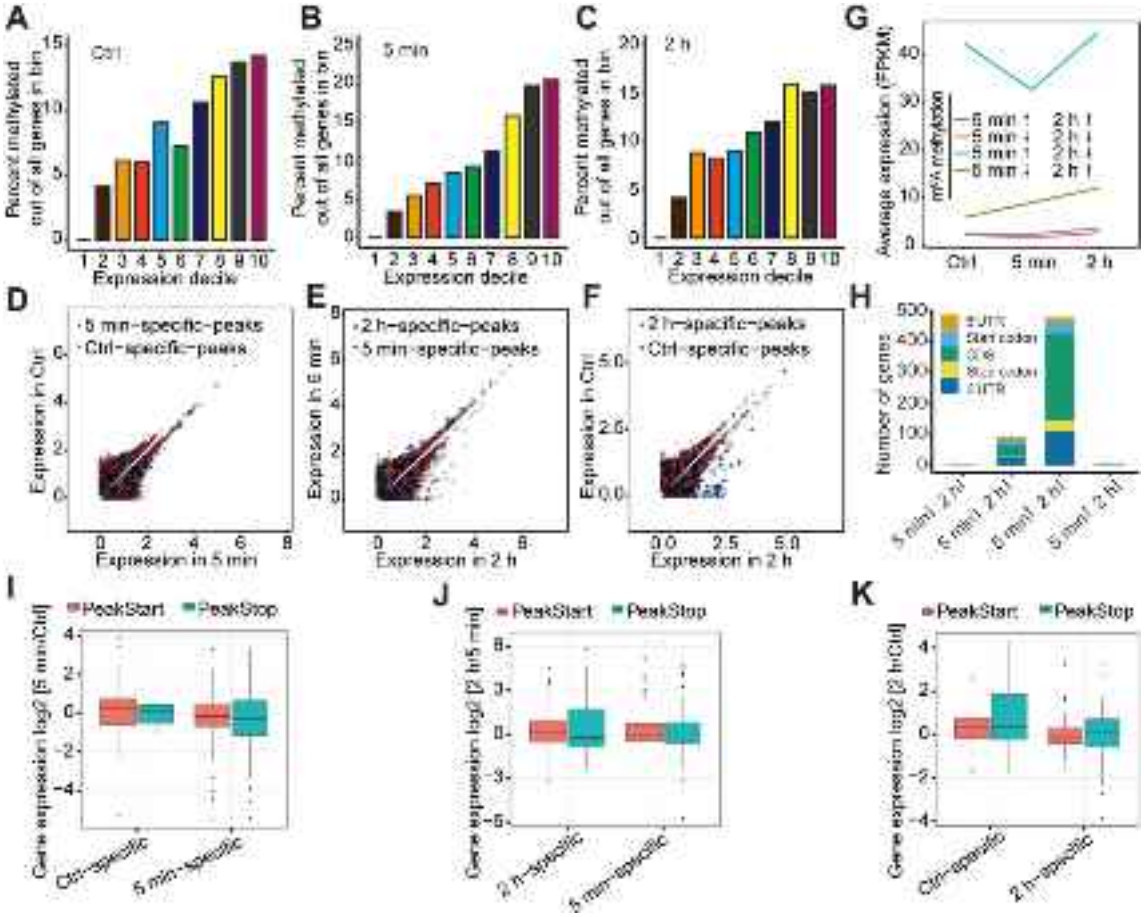

Fig. 7. Correlation analyses between mRNA m^{6}A methylation and gene expression. (A–C) The relationship between relative expression levels and m^{6}A methylation rates of genes at 0 min (A), 5 min (B) and 2 h (C) postirradiation. (D–F) Differentially expressed mRNAs with time-specific m^{6}A peaks in each pairwise comparison of 5 min vs Ctrl (D), 2 h vs 5 min (E), or 2 h vs Ctrl (F). (G) The average expression patterns over time, according to fragments per kilobase of transcript per million mapped reads (FPKM), of mRNAs with m^{6}A methylation patterns of (5 min_up/2 h_up), (5 min_down/2 h_down), (5 min_up/2 h_down) and (5 min_down/2 h_up). (H) Respective numbers of genes with the mRNA methylation profiles of (5 min_up/2 h_up), (5 min_down/2 h_down), (5 min_up/2 h_down) and (5 min_down/2 h_up). A stacked bar plot was used to show the gene numbers corresponding to each section (5′UTR, start codon, CDS, stop codon and 3′UTR) of transcripts. (I–K) The relative expression levels of genes containing time-specific m^{6}A peaks were compared between every two time points (5 min/Ctrl (I), 2 h/5 min (J) and 2 h/Ctrl (K)), in which the relationships between the peak positions (5′- or 3'-) and expression levels are shown.

m^{6}A modification is a new regulator for radiation stimulation (Fig. 7D–F, Data S21). Although there was no consistent correlation between the time-course patterns of m^{6}A methylation and gene expression, mRNAs with reversible m^{6}A methylation tendencies ((5 min_up/2 h_down) and (5 min_down/2 h_up)) corresponded to relatively higher average expression levels (Fig. 7G). Moreover, the reversible m^{6}A methylation profile after γ-ray exposure predicted far more genes than the continuously evolving profiles, similar to Fig. 4I, and most genes in the (5 min_up/2 h_down) group exhibited preferable m^{6}A enrichment in the CDS region (Fig. 7H, Data S22). Then, we analyzed whether the expression levels of m^{6}A-containing genes correlated with the peak positions by dividing each moment-specific m^{6}A-bearing gene into two categories (the 5′ m^{6}A-containing genes (peak start) and 3′ m^{6}A-containing genes (peak stop)). The data showed that, on the one hand, in the comparisons of 5 min/Ctrl and 2 h/5 min, the peak start m^{6}A peaks showed slightly higher expression levels of most time-specific genes, which was different from the 2 h/Ctrl comparison; on the other hand, both the peak start and peak stop m^{6}A peaks in the Ctrl-specific cluster predicted relatively higher expression levels of genes than those in the 5 min-specific or 2 h-specific cluster, while there was less difference in the expression levels of m^{6}A-containing genes between the 2 h-specific and 5 min-specific groups (Fig. 7I–K). Taken together, the gene expression levels are correlated with m^{6}A-modifying characteristics in some aspects, including the methylation ratio, time-dependent evolving patterns and peak locations.

3.8. Blocking m^{6}A catalytic enzyme expression in vivo leads to alterations in mouse radiosensitivity

To validate whether mRNA m^{6}A methylation impacts the radiosensitivity of mouse models, *METTL3* and *FTO* were interfered with *in vivo* by injecting 5 nmol/20 g animal-applicable siRNAs (Gong et al., 2019; Krutzfeldt et al., 2005; Wang et al., 2020), through the mouse tail vein just before radiation challenge. The siRNA injection was repeated once after three days. Firstly, the interference efficiency was verified at day 3 and day 7 both at the mRNA and protein levels (Fig. 8A–D, Fig. S5A-D). After 4 Gy γ-irradiation, mice with *METTL3* or *FTO* silencing showed higher body weights at some time points (Fig. 8E). In detail, si*FTO* treatment improved radiation-impaired hemogram indexes but lightened the weights of hematogenic organs in irradiated mice (Fig. 8F–H, Fig. S5E and F). However, si*METTL3* treatment rescued the TBI-induced thymus weight reduction (Fig. S8F). Additionally, the TBI + si*FTO* group showed an increase in body weights compared with the TBI group under 7.2 Gy (which was the medial lethal dose in mice) γ-irradiation (Fig. S5G), and there was no significant discrepancy in the survival rates among the three groups (Fig. S5H). The preliminary blocking explorations suggest that disturbing the expression of m^{6}A-related enzymes alters the sensitivities of mouse models to γ-irradiation in multiple aspects. The data hint that *in vivo* si*FTO* treatment may relieve the TBI-induced physical condition impairment, of which the efficacy may be better than si*METTL3* treatment. To further explore the role of RNA m^{6}A modification in the recovery process after γ-irradiation, we assessed the effects of double interfering with the two "erasers" *FTO* and *ALKBH5* on the radiosensitivity of mice. The interference efficiency was also verified at day 3 and day 7 at the mRNA and protein levels (Fig. 8I-L, Fig. S5I-L). As expected, double interfering with *FTO* and *ALKBH5* improved the physical condition of TBI-treated mice in multiple aspects, as judged by the amelioration of body weight (Fig. 8M), hemogram indexes (WBC (Fig. 8N), lymphocyte (Fig. 8O), lymphocyte% (Fig. 8P), RBC (Fig. 8Q), PLT (Fig. 8R), HGB (Fig. S5M)) and the weights of hematogenic organ spleen and thymus (Fig. 8S and T). Additionally, the percentage of hematopoietic stem cells (HSCs) and hematopoietic progenitor cells (HPCs) in bone marrow cell population both elevated in TBI + si*FTO* + si*ALKBH5* group (Fig. 8U, Fig. S5N and O). Collectively, the data preliminarily suggest that disturbing the expression of m^{6}A demethylases ameliorates radiation hematopoietic injury. Our observations demonstrate that mRNA m^{6}A modification of bone marrow plays a key role in the hematopoietic recovery after radiation exposure.

4. Discussion

Accidental ionizing radiation following radionuclide release, such as in Chernobyl and Fukushima Nuclear Power Plant, drives acute or chronic radiation injuries to living beings (Tagami et al., 2011; Zablotska et al., 2011). Iatrogenic irradiation, such as radiotherapy for cancers, also indirectly subjects local normal tissues or even distal organs to unexpected radiation infringement. Except the well-known DNA double-strand breaking, the deficiency of theoretical innovation for further mechanisms underlying radiation toxicity leads to the technological hysteresis of repairing and rescuing for irradiation injury. Heretofore, amifostine is the only well-proven drug used for radiation injury treatment, but its application is limited due to the inconvenient administration of injection delivery and the existence of strong side effects (Yu et al., 2020). Accordingly, prevention and curing radiation-induced injuries remain conundrums and require breakthroughs in both fundamental and application research. The hematopoietic system is the most sensitive organ to irradiation. TBI with the dose higher than 3.5 Gy causes severe injury and persistent myelosuppression (Shao et al., 2014; Zhang et al., 2019). Hematopoietic toxicity is the main pathological basis of acute radiation syndrome. Impairments in hematopoietic organs appear at the early stage after irradiation and have obvious time-dependent characteristics, which dictate taxonomic diagnosis and prognosis prediction (Micewicz et al., 2019). In agreement with the evidence, TBI atrophied the thymus and spleen and harmed the hemogram within 2 h in our study. Importantly, TBI exposure altered the RNA m^{6}A content and the expression levels of m^{6}A modification related enzymes within 2 h following irradiation. The results suggest that m^{6}A modification responds to radiation stimuli rapidly and might play key roles in the development of radiation toxicity.

With the mystery of epigenetics unveiled, researchers began to realize the significance of RNA epigenetic modifications in the post-transcriptomic network. RNA epigenetic information is controlled by the genome sequence, environmental exposure, and stochasticity or random chance (Golson and Kaestner, 2017; Tammen et al., 2013). As such, epitranscriptomics stands at the interface of the transcriptome, development, and environmental exposure (Feinberg, 2018). As the most pervasive and conserved transcriptional modification within eukaryotic RNAs, m^{6}A modification and the related catalytic enzymes participate in versatile life activities and diseases (Hao et al., 2019; Hu et al., 2020; Li et al., 2018; Richard et al., 2019; Song et al., 2020; Su et al., 2020; Yang et al., 2020; Yoon et al., 2017; Zhao et al., 2014). The variable modificatory m^{6}A status responds to temporal and spatial transition and fluctuates with homeostatic state and external environmental challenges (Dorn et al., 2019; Engel et al., 2018; Xiang et al., 2017). An enrichment near the CDS region of genes has implicated m^{6}A in transcript processing, translational regulation and other mechanisms to relate this modification to development, differentiation and oncogenesis (Liu et al., 2019; Saletore et al., 2013; Wu et al., 2019; Zhang et al., 2020a). Intriguingly, there was an overt preference of the enrichment region in the CDS for m^{6}A upregulation peaks at 5 min. The m^{6}A modificatory profile experienced a "change then recover" tendency following irradiation; as a whole, γ-irradiation was mainly upregulated, rather than downregulated.

Recent studies have discovered dynamic and reversible deposition of m^{6}A on mRNA and other types of nuclear RNA (Fu et al., 2014; Yu et al., 2018). Here, we also uncovered the "change then recover" mode of m^{6}A modification in poly(A)-RNA after γ-irradiation treatment from multiple aspects, for example, from m^{6}A abundance, spatial distribution, fold enrichment in different regions and the mRNA expression of effector enzymes. This epigenetic modification was sensitive to irradiation stimulation and achieved the "change then recover" tendency in 2 h. Additionally, some studies reported that the differential m^{6}A

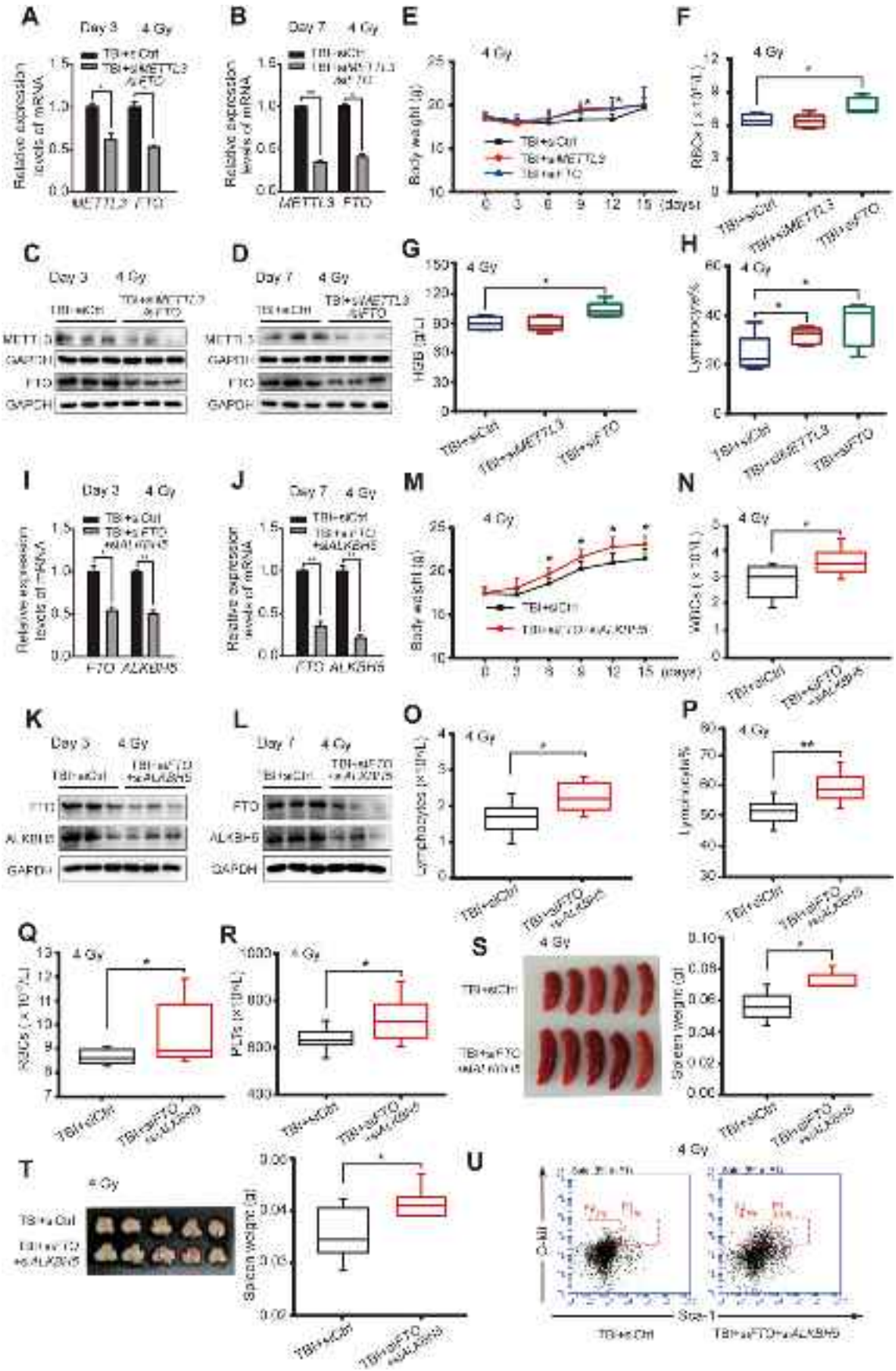

(caption on next page)

Fig. 8. Blocking m^{6}A catalytic enzyme expression *in vivo* leads to alterations in mouse radiosensitivity. Before irradiation began, the animal-applicable siRNAs modified by 2′OMe+5′ Chol perssad, targeting *METTL3* or *FTO*, were injected into the mouse tail vein at a dose of 5 nmol/20 g, and an equivalent volume of normal saline containing dissolved scrambled siRNA was injected as a control. (A–B) The interference efficiency of the siRNAs in bone marrow cells at day 3 and day 7 after the treatment was determined by qRT-PCR for the mRNA level. (n = 12). (C–D) The interference efficiency of the siRNAs in bone marrow cells at day 3 and day 7 after the treatment was determined by Western blot for the protein level. (n = 3, 1 replicate consisted of a mixture of bone marrow cells from every four mice in one group). (E)The body weights of mice in the TBI + siCtrl/TBI + si*METTL3*/TBI + si*FTO* groups 15 days after 4 Gy γ-irradiation. (n = 12). (F–H) Certain hemogram indexes, including red blood cells (RBCs, F), hemoglobin (HGB, G) and lymphocyte% (H), were determined on the 15th day of 4 Gy γ-irradiation. (n = 12). Before irradiation began, a mixture of animal-applicable siRNAs targeting *FTO* and *ALKBH5* were injected into the mouse tail vein at a dose of 5 nmol/20 g, and an equivalent volume of normal saline containing dissolved scrambled siRNA was injected as a control. (I–J) The interference efficiency of the siRNAs in bone marrow cells at day 3 and day 7 after the treatment was determined by qRT-PCR for the mRNA level. (n = 12). (K–L) The interference efficiency of the siRNAs in bone marrow cells at day 3 and day 7 after the treatment was determined by Western blot for the protein level. (n = 3, 1 replicate consisted of a mixture of bone marrow cells from every four mice in one group). (M)The body weights of mice in the TBI + siCtrl/TBI + si*FTO* + si*ALKBH5* groups 15 days after 4 Gy γ-irradiation. (n = 12). (N–R) Certain hemogram indexes, including white blood cells (WBCs, N), lymphocytes (O), lymphocyte% (P), red blood cells (RBCs, Q) and platelet (PLT, R), were determined by a blood cell counter on the 15th day of 4 Gy γ-irradiation. (n = 12). (S–T) Images and weights of the spleen (S) or thymus (T) of the two groups on the 15th day of 4 Gy γ-irradiation. (n = 12). (U) Representative fluorescence-activated cell sorting (FACS) plots of hematopoietic progenitor cells (HPCs) and hematopoietic stem cells (HSCs). The percentage of HPCs and HSC cells in lineage-negative cells were analyzed using FACS assay at day 15 after 4 Gy TBI for the mice in TBI + siCtrl/TBI + si*FTO* + si*ALKBH5* groups. (n = 12). Data are shown as the mean ± SEM of three independent experiments. Statistically significant differences are indicated: *, $P < 0.05$; **, $P < 0.01$; Student's *t*-test. N.S., no significance. (For interpretation of the references to color in this figure legend, the reader is referred to the Web version of this article.)

methylation peaks might be the consequent of the differential mRNA expression levels (Lu et al., 2021; McIntyre et al., 2020). We analyzed differential calling peaks obtained from the IP samples for the variation tendency in corresponding Input samples, and the result exhibited no obvious similarity for the trend between IP and Input samples. That might partly be related to the three replicates set in each group, and the differential peaks were merged from the replicates. Notably, there is indeed correlations between m^{6}A peaks and mRNA expression levels, the functional studies of m^{6}A demonstrate that m^{6}A modification regulates the lifetime of mRNA and thereby influences the expression levels (Anders et al., 2015; Wang et al., 2014; Wang et al., 2015). In the future, mature sophisticated algorithm and strategy are required to precisely elucidate the relationship between epigenetic modifications and modulation of gene expression.

In light of our data, modulation of m^{6}A modifications might impact the development of radiation toxicity. Thus, we interfered with the expression levels of m^{6}A catalytic enzymes *in vivo* and found that blocking the expression of m^{6}A catalytic enzymes *in vivo* led to alterations of mouse radiosensitivity in multiple aspects. Silencing of the m^{6}A demethylase *FTO* and *ALKBH5* ameliorated radiation hematopoietic injury. Additionally, the LC-MS/MS assay revealed a reduction of global m^{6}A content 2 h after irradiation. The results preliminarily suggest that TBI treatment suppresses the comprehensive m^{6}A levels in bone marrow at the early stage, and knockdown the m^{6}A demethylase expression to rescue the irradiation-induced m^{6}A decline contributes to the recovery of radiation exposure.

In future studies, key target mRNAs and m^{6}A sites should be precisely identified, reliable m^{6}A spectra varying with time should be obtained, and interfering approaches towards target mRNAs and m^{6}A effector enzymes *in vitro* and *in vivo* should be well verified and then applied. All of these explorations need to be tried in further investigations.

5. Conclusion

In summary, we depicted the global and dynamic m^{6}A modification landscape and transcriptome alterations of mouse bone marrow in γ-irradiation-induced hematopoietic deficiency and revealed the "change then recover" characteristics of the mRNA m^{6}A methylome. Notably, blocking the m^{6}A catalytic enzymes *in vivo* leads to alterations in mouse radiosensitivity. Our study provides a theoretical foundation for intervening in the radiation crisis at the m^{6}A epigenetic level and thereby sheds light on the roles of epitranscriptomes in the mammalian response to radiation.

CRediT author contribution statement

Shuqin Zhang: Data curation, Formal analysis, Funding acquisition, Investigation, Project administration, Software, Validation, Writing-original draft, Writing-review & editing, Conceptualization. **Jiali Dong**: Data curation, Formal analysis, Software, Visualization, Writing-review & editing. **Yuan Li:** Data curation, Formal analysis, Visualization, Writing-review & editing. **Huiwen Xiao:** Data curation, Formal analysis, Visualization, Writing-review & editing. **Yue Shang:** Data curation, Formal analysis, Investigation. **Bin Wang:** Data curation, Writing-review & editing. **Zhiyuan Chen:** Formal analysis, Visualization, Writing-review & editing. **Mengran Zhang:** Formal analysis, Software. **Saijun Fan:** Conceptualization, Funding acquisition, Supervision, Methodology. **Ming Cui:** Conceptualization, Data curation, Investigation, Funding acquisition, Methodology, Project administration, Supervision, Validation, Writing-review & editing.

Declaration of competing interest

The authors declare that they have no known competing financial interests or personal relationships that could have appeared to influence the work reported in this paper.

Acknowledgements

This work was supported by grants from the National Natural Science Foundation of China (No. 81803062, 81872555, 81730086 and 81572969), CAMS Innovation Fund for Medical Sciences (CIFMS, 2016-I2M-1–017 and 2017-I2M-B&R-13), the Technology and Development and Research Projects for Research Institutes, Ministry of Science and Technology (2014EG150134), the Tianjin Science and Technology Support Plan Project (TJKJZC, 14ZCZDSY00001) and the Drug Innovation Major Project of China (2018ZX09711001-007-008).

Appendix A. Supplementary data

Supplementary data to this article can be found online at https://doi.org/10.1016/j.envpol.2021.117509.

References

Alarcon, C.R., Lee, H., Goodarzi, H., Halberg, N., Tavazoie, S.F., 2015. N6-methyladenosine marks primary microRNAs for processing. Nature 519, 482–485.
Amort, T., Rieder, D., Wille, A., Khokhlova-Cubberley, D., Riml, C., Trixl, L., Jia, X.Y., Micura, R., Lusser, A., 2017. Distinct 5-methylcytosine profiles in poly(A) RNA from mouse embryonic stem cells and brain. Genome Biol. 18, 1.
Anastassopoulou, J., Theophanides, T., 2002. Magnesium-DNA interactions and the possible relation of magnesium to carcinogenesis. Irradiation and free radicals. Crit. Rev. Oncol.-Hematol. 42, 79–91.
Anders, S., Pyl, P.T., Huber, W., 2015. HTSeq–a Python framework to work with high-throughput sequencing data. Bioinformatics 31, 166–169.

Chen, X.Y., Zhang, J., Zhu, J.S., 2019. The role of m(6)A RNA methylation in human cancer. Mol. Canc. 18, 103.
Chi, H.C., Tsai, C.Y., Tsai, M.M., Lin, K.H., 2018. Impact of DNA and RNA methylation on radiobiology and cancer progression. Int. J. Mol. Sci. 19.
Dainiak, N., Sorba, S., 1997. Early identification of radiation accident victims for therapy of bone marrow failure. Stem Cell. 15 (Suppl. 2), 275–285.
De Jesus, D.F., Kulkarni, R.N., 2019. Omics" and "epi-omics" underlying the beta-cell adaptation to insulin resistance. Mol. Metabol. 27S, S42–S48.
Desrosiers, R., Friderici, K., Rottman, F., 1974. Identification of methylated nucleosides in messenger RNA from Novikoff hepatoma cells. Proc. Natl. Acad. Sci. U. S. A 71, 3971–3975.
Dominissini, D., Moshitch-Moshkovitz, S., Schwartz, S., Salmon-Divon, M., Ungar, L., Osenberg, S., Cesarkas, K., Jacob-Hirsch, J., Amariglio, N., Kupiec, M., et al., 2012. Topology of the human and mouse m6A RNA methylomes revealed by m6A-seq. Nature 485, 201–206.
Dorn, L.E., Tual-Chalot, S., Stellos, K., Accornero, F., 2019. RNA epigenetics and cardiovascular diseases. J. Mol. Cell. Cardiol. 129, 272–280.
Engel, M., Eggert, C., Kaplick, P.M., Eder, M., Roh, S., Tietze, L., Namendorf, C., Arloth, J., Weber, P., Rex-Haffner, M., et al., 2018. The role of m(6)A/m-RNA methylation in stress response regulation. Neuron 99, 389–403 e389.
Feinberg, A.P., 2018. The key role of epigenetics in human disease prevention and mitigation. N. Engl. J. Med. 378, 1323–1334.
Frye, M., Harada, B.T., Behm, M., He, C., 2018. RNA modifications modulate gene expression during development. Science 361, 1346–1349.
Fu, Y., Dominissini, D., Rechavi, G., He, C., 2014. Gene expression regulation mediated through reversible m(6)A RNA methylation. Nat. Rev. Genet. 15, 293–306.
Golson, M.L., Kaestner, K.H., 2017. Epigenetics in formation, function, and failure of the endocrine pancreas. Mol. Metabol. 6, 1066–1076.
Gong, Y., Li, S.J., Liu, R., Zhan, J.F., Tan, C., Fang, Y.F., Chen, Y., Yu, B., 2019. Inhibition of YAP with siRNA prevents cartilage degradation and ameliorates osteoarthritis development. J. Mol. Med. 97, 103–114.
Guo, X., Li, K., Jiang, W., Hu, Y., Xiao, W., Huang, Y., Feng, Y., Pan, Q., Wan, R., 2020. RNA demethylase ALKBH5 prevents pancreatic cancer progression by posttranscriptional activation of PER1 in an m6A-YTHDF2-dependent manner. Mol. Canc. 19, 91.
Hao, H., Hao, S., Chen, H., Chen, Z., Zhang, Y., Wang, J., Wang, H., Zhang, B., Qiu, J., Deng, F., et al., 2019. N6-methyladenosine modification and METTL3 modulate enterovirus 71 replication. Nucleic Acids Res. 47, 362–374.
He, L., Li, H., Wu, A., Peng, Y., Shu, G., Yin, G., 2019. Functions of N6-methyladenosine and its role in cancer. Mol. Canc. 18, 176.
Hu, Y., Ouyang, Z., Sui, X., Qi, M., Li, M., He, Y., Cao, Y., Cao, Q., Lu, Q., Zhou, S., et al., 2020. Oocyte competence is maintained by m(6)A methyltransferase KIAA1429-mediated RNA metabolism during mouse follicular development. Cell Death Differ. 27, 2468–2483.
Jabs, S., Biton, A., Becavin, C., Nahori, M.A., Ghozlane, A., Pagliuso, A., Spano, G., Guerineau, V., Touboul, D., Giai Gianetto, Q., et al., 2020. Impact of the gut microbiota on the m(6)A epitranscriptome of mouse cecum and liver. Nat. Commun. 11, 1344.
Krutyholowa, R., Hammermeister, A., Zabel, R., Abdel-Fattah, W., Reinhardt-Tews, A., Helm, M., Stark, M.J.R., Breunig, K.D., Schaffrath, R., Glatt, S., 2019. Kti12, a PSTK-like tRNA dependent ATPase essential for tRNA modification by Elongator. Nucleic Acids Res. 47, 4814–4830.
Krutzfeldt, J., Rajewsky, N., Braich, R., Rajeev, K.G., Tuschl, T., Manoharan, M., Stoffel, M., 2005. Silencing of microRNAs in vivo with 'antagomirs'. Nature 438, 685–689.
Li, M., Zhao, X., Wang, W., Shi, H., Pan, Q., Lu, Z., Perez, S.P., Suganthan, R., He, C., Bjoras, M., et al., 2018. Ythdf2-mediated m(6)A mRNA clearance modulates neural development in mice. Genome Biol. 19, 69.
Liu, L., Wang, J., Sun, G., Wu, Q., Ma, J., Zhang, X., Huang, N., Bian, Z., Gu, S., Xu, M., et al., 2019. m(6)A mRNA methylation regulates CTNNB1 to promote the proliferation of hepatoblastoma. Mol. Canc. 18, 188.
Liu, Q., Gregory, R.I., 2019. RNAmod: an integrated system for the annotation of mRNA modifications. Nucleic Acids Res. 47, W548–W555.
Lu, Z., Liu, J., Yuan, C., Jin, M., Quan, K., Chu, M., Wei, C., 2021. m(6)A mRNA methylation analysis provides novel insights into heat stress responses in the liver tissue of sheep. Genomics 113, 484–492.
Lu, Z., Ma, Y., Li, Q., Liu, E., Jin, M., Zhang, L., Wei, C., 2019. The role of N(6)-methyladenosine RNA methylation in the heat stress response of sheep (Ovis aries). Cell Stress Chaperones 24, 333–342.
Ma, C., Chang, M., Lv, H., Zhang, Z.W., Zhang, W., He, X., Wu, G., Zhao, S., Zhang, Y., Wang, D., et al., 2018. RNA m(6)A methylation participates in regulation of postnatal development of the mouse cerebellum. Genome Biol. 19, 68.
McIntyre, A.B.R., Gokhale, N.S., Cerchietti, L., Jaffrey, S.R., Horner, S.M., Mason, C.E., 2020. Limits in the detection of m(6)A changes using MeRIP/m(6)A-seq. Sci. Rep. 10, 6590.
Meyer, K.D., Jaffrey, S.R., 2017. Rethinking m(6)A readers, writers, and erasers. Annu. Rev. Cell Dev. Biol. 33, 319–342.
Micewicz, E.D., Iwamoto, K.S., Ratikan, J.A., Nguyen, C., Xie, M.W., Cheng, G., Boxx, G. M., Deriu, E., Damoiseaux, R.D., Whitelegge, J.P., et al., 2019. The aftermath of surviving acute radiation hematopoietic syndrome and its mitigation. Radiat. Res. 191, 323–334.
Mishra, B., Luderer, U., 2019. Reproductive hazards of space travel in women and men. Nat. Rev. Endocrinol. 15, 713–730.
Muller, S., Glass, M., Singh, A.K., Haase, J., Bley, N., Fuchs, T., Lederer, M., Dahl, A., Huang, H., Chen, J., et al., 2019. IGF2BP1 promotes SRF-dependent transcription in cancer in a m6A- and miRNA-dependent manner. Nucleic Acids Res. 47, 375–390.
Nikjoo, H., Emfietzoglou, D., Liamsuwan, T., Taleei, R., Liljequist, D., Uehara, S., 2016. Radiation track, DNA damage and response-a review. Rep. Progr. Phys. Phys. Soc. 79, 116601.
Ontiveros, R.J., Stoute, J., Liu, K.F., 2019. The chemical diversity of RNA modifications. Biochem. J. 476, 1227–1245.
Patil, D.P., Chen, C.K., Pickering, B.F., Chow, A., Jackson, C., Guttman, M., Jaffrey, S.R., 2016. m(6)A RNA methylation promotes XIST-mediated transcriptional repression. Nature 537, 369–373.
Richard, E.M., Polla, D.L., Assir, M.Z., Contreras, M., Shahzad, M., Khan, A.A., Razzaq, A., Akram, J., Tarar, M.N., Blanpied, T.A., et al., 2019. Bi-allelic variants in METTL5 cause autosomal-recessive intellectual disability and microcephaly. Am. J. Hum. Genet. 105, 869–878.
Robinson, M., Shah, P., Cui, Y.H., He, Y.Y., 2019. The role of dynamic m(6) A RNA methylation in photobiology. Photochem. Photobiol. 95, 95–104.
Roundtree, I.A., Evans, M.E., Pan, T., He, C., 2017. Dynamic RNA modifications in gene expression regulation. Cell 169, 1187–1200.
Saletore, Y., Chen-Kiang, S., Mason, C.E., 2013. Novel RNA regulatory mechanisms revealed in the epitranscriptome. RNA Biol. 10, 342–346.
Shao, L., Luo, Y., Zhou, D., 2014. Hematopoietic stem cell injury induced by ionizing radiation. Antioxidants Redox Signal. 20, 1447–1462.
Song, H., Feng, X., Zhang, H., Luo, Y., Huang, J., Lin, M., Jin, J., Ding, X., Wu, S., Huang, H., et al., 2019. METTL3 and ALKBH5 oppositely regulate m(6)A modification of TFEB mRNA, which dictates the fate of hypoxia/reoxygenation-treated cardiomyocytes. Autophagy 15, 1419–1437.
Song, H., Wang, L., Chen, D., Li, F., 2020. The function of pre-mRNA alternative splicing in mammal spermatogenesis. Int. J. Biol. Sci. 16, 38–48.
Su, R., Dong, L., Li, Y., Gao, M., Han, L., Wunderlich, M., Deng, X., Li, H., Huang, Y., Gao, L., et al., 2020. Targeting FTO suppresses cancer stem cell maintenance and immune evasion. Canc. Cell 38, 79–96 e11.
Tagami, K., Uchida, S., Uchihori, Y., Ishii, N., Kitamura, H., Shirakawa, Y., 2011. Specific activity and activity ratios of radionuclides in soil collected about 20 km from the Fukushima Daiichi Nuclear Power Plant: radionuclide release to the south and southwest. Sci. Total Environ. 409, 4885–4888.
Taketo, K., Konno, M., Asai, A., Koseki, J., Toratani, M., Satoh, T., Doki, Y., Mori, M., Ishii, H., Ogawa, K., 2018. The epitranscriptome m6A writer METTL3 promotes chemo- and radioresistance in pancreatic cancer cells. Int. J. Oncol. 52, 621–629.
Tammen, S.A., Friso, S., Choi, S.W., 2013. Epigenetics: the link between nature and nurture. Mol. Aspect. Med. 34, 753–764.
Visvanathan, A., Patil, V., Arora, A., Hegde, A.S., Arivazhagan, A., Santosh, V., Somasundaram, K., 2018. Essential role of METTL3-mediated m(6)A modification in glioma stem-like cells maintenance and radioresistance. Oncogene 37, 522–533.
Wang, J., Wang, Y., Zhang, H., Chang, J., Lu, M., Gao, W., Liu, W., Li, Y., Yin, L., Wang, X., et al., 2020. Identification of a novel microRNA-141-3p/Forkhead box C1/beta-catenin axis associated with rheumatoid arthritis synovial fibroblast function in vivo and in vitro. Theranostics 10, 5412–5434.
Wang, X., Lu, Z., Gomez, A., Hon, G.C., Yue, Y., Han, D., Fu, Y., Parisien, M., Dai, Q., Jia, G., et al., 2014. N6-methyladenosine-dependent regulation of messenger RNA stability. Nature 505, 117–120.
Wang, X., Zhao, B.S., Roundtree, I.A., Lu, Z., Han, D., Ma, H., Weng, X., Chen, K., Shi, H., He, C., 2015. N(6)-methyladenosine modulates messenger RNA translation efficiency. Cell 161, 1388–1399.
Wu, R., Li, A., Sun, B., Sun, J.G., Zhang, J., Zhang, T., Chen, Y., Xiao, Y., Gao, Y., Zhang, Q., et al., 2019. A novel m(6)A reader Prrc2a controls oligodendroglial specification and myelination, *29*, 23–41.
Xiang, Y., Laurent, B., Hsu, C.H., Nachtergaele, S., Lu, Z., Sheng, W., Xu, C., Chen, H., Ouyang, J., Wang, S., et al., 2017. Corrigendum: RNA m(6)A methylation regulates the ultraviolet-induced DNA damage response. Nature 552, 430.
Yang, J., Liu, J., Zhao, S., Tian, F., 2020. N(6)-Methyladenosine METTL3 Modulates the proliferation and apoptosis of lens epithelial cells in diabetic cataract. Mol. Ther. Nucleic Acids 20, 111–116.
Yoon, K.J., Ringeling, F.R., Vissers, C., Jacob, F., Pokrass, M., Jimenez-Cyrus, D., Su, Y., Kim, N.S., Zhu, Y., Zheng, L., et al., 2017. Temporal control of mammalian cortical neurogenesis by m(6)A methylation. Cell 171, 877–889 e817.
Yu, J., Chen, M., Huang, H., Zhu, J., Song, H., Zhu, J., Park, J., Ji, S.J., 2018. Dynamic m6A modification regulates local translation of mRNA in axons. Nucleic Acids Res. 46, 1412–1423.
Yu, X., Li, M., Zhu, L., Li, J., Zhang, G., Fang, R., Wu, Z., Jin, Y., 2020. Amifostine-loaded armored dissolving microneedles for long-term prevention of ionizing radiation-induced injury. Acta Biomater. 112, 87–100.
Zablotska, L.B., Ron, E., Rozhko, A.V., Hatch, M., Polyanskaya, O.N., Brenner, A.V., Lubin, J., Romanov, G.N., McConnell, R.J., O'Kane, P., et al., 2011. Thyroid cancer risk in Belarus among children and adolescents exposed to radioiodine after the Chornobyl accident. Br. J. Canc. 104, 181–187.
Zhang, H., Shi, X., Huang, T., Zhao, X., Chen, W., Gu, N., Zhang, R., 2020a. Dynamic landscape and evolution of m6A methylation in human. Nucleic Acids Res. 48, 6251–6264.
Zhang, H., Zhai, Z., Wang, Y., Zhang, J., Wu, H., Wang, Y., Li, C., Li, D., Lu, L., Wang, X., et al., 2013. Resveratrol ameliorates ionizing irradiation-induced long-term hematopoietic stem cell injury in mice. Free Radic. Biol. Med. 54, 40–50.
Zhang, J., Han, X., Zhao, Y., Xue, X., Fan, S., 2019. Mouse serum protects against total body irradiation-induced hematopoietic system injury by improving the systemic environment after radiation. Free Radic. Biol. Med. 131, 382–392.
Zhang, L., Hou, C., Chen, C., Guo, Y., Yuan, W., Yin, D., Liu, J., Sun, Z., 2020b. The role of N(6)-methyladenosine (m(6)A) modification in the regulation of circRNAs. Mol. Canc. 19, 105.

Zhang, S., Zhao, B.S., Zhou, A., Lin, K., Zheng, S., Lu, Z., Chen, Y., Sulman, E.P., Xie, K., Bogler, O., et al., 2017. m(6)A Demethylase ALKBH5 maintains tumorigenicity of glioblastoma stem-like cells by sustaining FOXM1 expression and cell proliferation program. Canc. Cell 31, 591–606 e596.
Zhang, W., Song, M., Qu, J., Liu, G.H., 2018. Epigenetic modifications in cardiovascular aging and diseases. Circ. Res. 123, 773–786.
Zhang, Y., Martin, S.G., 2014. Redox proteins and radiotherapy. Clin. Oncol. 26, 289–300.
Zhao, B.S., Roundtree, I.A., He, C., 2017. Post-transcriptional gene regulation by mRNA modifications. Nat. Rev. Mol. Cell Biol. 18, 31–42.
Zhao, X., Yang, Y., Sun, B.F., Shi, Y., Yang, X., Xiao, W., Hao, Y.J., Ping, X.L., Chen, Y.S., Wang, W.J., et al., 2014. FTO-dependent demethylation of N6-methyladenosine regulates mRNA splicing and is required for adipogenesis. Cell Res. 24, 1403–1419.
Zhong, X., Yu, J., Frazier, K., Weng, X., Li, Y., Cham, C.M., Dolan, K., Zhu, X., Hubert, N., Tao, Y., et al., 2018. Circadian Clock Regulation of hepatic lipid metabolism by modulation of m(6)A mRNA methylation. Cell Rep. 25, 1816–1828 e1814.

1. Supplementary materials and methods

1.1 Animal care

Six- to eight-week-old male C57BL/6J mice were purchased from Beijing Huafukang Bioscience Co., Inc. (Beijing, China). Mice were housed in the specific pathogen-free (SPF) animal facility at the Institute of Radiation Medicine (IRM), Chinese Academy of Medical Sciences (CAMS). Mice were kept under standard conditions (ambient temperature 22±2 ℃, air humidity 40-70% and a 12/12-h light/dark cycle) with continuous access to food and water. Animal experiments were performed according to the institutional guidelines approved by the Animal Care and Ethics Committee of IRM-PUMC, which complied with the Guide for the Care and Use of Laboratory Animals and the National Institutes of Health Guide for the Care and Use of Laboratory Animals.

1.2 Experimental groups

(1) Control (Ctrl), 5 min and 2 h groups: healthy 6- to 8-week-old male C57BL/6J mice received no γ-ray exposure or 4 Gy γ-irradiation treatment and were sacrificed at 0, 5 min and 2 h after the exposure. For the initial investigation of the effect of γ-irradiation on hemopoietic system, (n=18), in other single radiation treatment groups, (n=12). (2) TBI+si*Ctrl/* TBI+si*METTL3/*TBI+si*FTO/*TBI+si*FTO*+si*ALKBH5* groups: healthy 6- to 8-week-old male C57BL/6J mice were injected with approximate 200 μL of normal saline containing dissolved animal-applicable scrambled siRNA or siRNA targeting METTL3/*FTO*/FTO+*ALKBH5*, which was modified by 2'OMe+5' Chol perssad to enhance the stability (Gong et al., 2019; Krutzfeldt et al., 2005; Wang et al., 2020), through the tail vein just before 4- or 7.2-Gy γ-irradiation treatment at the dose of 5 nmol/20 g. The siRNA injection was repeated once after three days. (n=12).

1.3 Sample collection

For determination of radiation effects on the hematopoietic system, mice were treated with or without 4 Gy total body irradiation (TBI). Five minutes or 2 h after irradiation, peripheral blood was extracted from the orbital sinus and collected in ethylenediaminetetraacetic acid K_3 tubes for detection of hemogram indexes. Then, the mice were sacrificed by cervical dislocation, and the spleens and thymuses were dissected for imaging and weight measurement. Bone marrow cells were isolated as previously reported (Zhang et al., 2016); briefly, the cells were collected by flushing both the tibias and femurs with sterile PBS. For sample preparation of MeRIP-seq, MeRIP-qPCR, LC-MS/MS and Western blot, bone marrow cells from every four mice in one group were mixed together to obtain the three replicates per group, followed by the total RNA or protein extraction.

1.4 Determination of hemogram indexes

Peripheral blood obtained from the orbital sinus was analyzed on a hematology analyzer (Nihon Kohden, Japan). The quantification included white blood cell (WBC), lymphocyte%, monocyte%, granulocyte%, mean corpuscular hemoglobin concentration (MCHC), red blood cell (RBC), hemoglobin (HGB), platelet (PLT) and plateletcrit% (PCT%).

1.5 Quantification of IL-6 and TNF-α by ELISA

The thymus tissues were weighed and ground in proportional saline and centrifuged for 10 min at 1000 g, 4 ℃. Sample dilutions of 1:4 were used for the determination of the IL-6 and TNF-α levels using commercial ELISA kits (Mlbio, Shanghai, China) according to the manufacturer's protocol. The optical density was read at 450 nm (Rayto, Shenzhen, China).

1.6 Determination of the MDA levels

The MDA content levels in the spleen were measured using a specific MDA assay kit (Cat. No. BC0025, Solarbio, China) according to the manufacturer's instructions. After the indicated treatment, the absorbance was measured at 450 nm, 532 nm and 600 nm wavelengths by a microplate reader (DTX 880 Multimode Detector, Beckman Coulter, USA) and quantified according to the indicated equation in the protocol. The MDA content is presented as nmol/g.

1.7 LC-MS/MS analysis of m^6A content

Total RNA of bone marrow cells was extracted using TRIzol reagent (Invitrogen, USA) following to the manufacturer's instruction. 1 μg of total RNA was digested by 4 μl nuclease P1 (Sigma, USA) in 40 μL buffer solution (10 mM Tris-HCl pH 7.0, 100 mM NaCl, 2.5 mM $ZnCl_2$) at 37 °C for 12 h, followed by incubating with 1 μL alkaline phosphatase (Sigma, USA) at 37 °C for 2 h. Then the sample was extracted with chloroform and the upper aqueous solution was taken. RNA solution was concentrated and redissolved with ultrapure water for LC-ESI-MS/MS analysis. The nucleosides were separated by reverse phase high-performance liquid chromatography on an Agilent C18 column, coupled with mass spectrometry detection using AB SCIEX QTRAP 6500+. The m^6A levels were calculated as the ratio of m^6A to A based on the standard curve obtained from pure nucleoside standards running with the same batch of samples.

1.8 Quantitative reverse transcription real-time PCR (qRT-PCR) for monitoring the expression of m^6A regulating enzymes

Total RNA was extracted from bone marrow using TRIzol reagent (Invitrogen Corporation, CA, USA). Complementary DNA was synthesized from total RNA using poly(A)-tailed total RNA and reverse transcription primers with ImPro-II Reverse Transcriptase (Promega,

Madison, WI) according to the manufacturer's protocol. QRT-PCR monitoring of the expression levels of five m^6A effector enzymes, *METTL3*, *METTL14*, *WTAP*, *FTO* and *ALKBH5* was performed according to the instructions of Fast Start Universal SYBR Green Master (Rox) (Roche Diagnostics GmbH, Mannheim, Germany). Experiments were conducted in duplicate in three independent assays. Relative transcriptional fold changes were calculated as $2^{-\Delta\Delta Ct}$. GAPDH was used as an internal control for normalization. All primers are listed in Supplementary Table S1.

1.9 Protein extraction and Western blot analysis

Total proteins were extracted from the cells using radio immunoprecipitation assay (RIPA, Solarbio, China) buffer according to the manufacturer's protocol. Western blot analysis protocol was described previously (Zhang et al., 2017). The rabbit polyclonal primary antibodies to examine the protein expression levels of *METTL3*, *METTL14*, *WTAP*, *FTO* and *ALKBH5* were purchased from Proteintech, China. The mouse anti-GAPDH monoclonal antibody was purchased from abcam, England.

1.10 RNA isolation for MeRIP-seq

For each group, nine biological replicates were selected, of which every three replicates were combined into one replicate. Then, total RNA of bone marrow was extracted using TRIzol reagent (Invitrogen Corporation, CA, USA) in accordance with the manufacturer's instructions. The Ribo-Zero rRNA Removal Kit (Illumina, Inc., CA, USA) was used to remove the ribosomal RNA content of total RNAs. Then, the RNA was chemically fragmented into fragments of approximately 100 nucleotides in length using fragmentation buffer (Illumina, Inc.).

1.11 MeRIP-seq library construction and sequencing

MeRIP-Seq was performed by Cloudseq Biotech, Inc. (Shanghai, China) following a previously reported procedure with a few modifications (Luo et al., 2019; Meyer et al., 2012). In brief, RNA fragments were incubated with an anti-m^{6}A polyclonal antibody (202003; Synaptic Systems, Göttingen, Germany) in immunoprecipitation (IP) buffer for 2 h at 4°C. Then, the mixture was immunoprecipitated through incubation with protein-A beads (Thermo Fisher Scientific, MA, USA) for 2 h at 4 °C. Next, bound RNA with m^{6}A modifications (BERRY & ASSOCIATES, PR3732, MI, USA) was eluted from the beads in IP buffer, followed by subsequent extraction with TRIzol reagent (Thermo Fisher Scientific). Purified RNA was then collected for RNA-seq library construction with the NEBNextR Ultra™ RNA Library Prep Kit (New England Biolabs, MA, USA). Both m^{6}A IP samples and the input samples without IP were subjected to 150-bp paired-end sequencing on an Illumina HiSeq 4000 sequencer (Illumina, Inc.).

1.12 Library preparation for transcriptome sequencing

A total amount of 3 μg RNA per sample was used as input material for the RNA sample preparations. Sequencing libraries were generated using the NEBNext Ultra™ RNA Library Prep Kit for Illumina (NEB, USA) following the manufacturer's recommendations, and index codes were added to attribute sequences to each sample. Briefly, mRNA was purified from total RNA using poly-T oligo-attached magnetic beads. Fragmentation was carried out using divalent cations under elevated temperature in NEBNext First Strand Synthesis Reaction Buffer (5×). First strand cDNA was synthesized using random hexamer primers and M-MuLV Reverse Transcriptase (RNase H-treated). Second strand cDNA synthesis was subsequently performed using DNA Polymerase I and RNase H. The remaining overhangs were converted into blunt

ends *via* exonuclease/polymerase activities. After adenylation of the 3' ends of DNA fragments, NEBNext adaptors with hairpin loop structures were ligated to prepare for hybridization. To preferentially select cDNA fragments 250~300 bp in length, the library fragments were purified with the AMPure XP system (Beckman Coulter, Beverly, USA). Then, 3 μL USER Enzyme (NEB, USA) was used with size-selected, adaptor-ligated cDNA at 37 °C for 15 min followed by 5 min at 95 °C before PCR. Then, PCR was performed with Phusion High-Fidelity DNA polymerase, universal PCR primers and Index (X) Primer. Finally, the PCR products were purified (AMPure XP system), and library quality was assessed on an Agilent Bioanalyzer 2100 system.

1.13 Identification of methylation regions and detection of differential methylation regions

The software macs2 callpeak was used to identify the methylation regions in each sample. For detection of differential methylation regions, special scripts were compiled and conducted as follows. Merge peaks from different comparison groups were acquired, and the number and reads per million (RPM) values of the merge peaks in each sample or group were calculated. Then the ratio of RPM_{IP}/RPM_{Input} was used as foldenrichment, the foldchange value was obtained according to the ratio of foldenrichment between two independent groups. Log_2 foldchange >1 or <-1 is regarded as the threshold of the region defined as differential methylation region. The list of differential methylation regions were presented as Data S10.

1.14 Motif analysis

The interactions between transcription factors or chromatin histone modifications and DNA were not random, but they showed some specific sequence preference. MEME (Bailey et al., 2009; Bailey et al., 2015) and DREME (Bailey, 2011; Machanick and Bailey, 2011) were used

to detect the sequence motif, which determined the detection of long and short consensus sequences. After motif detection, Tomtom software (Gupta et al., 2007) was used to annotate the motifs based on sequence similarity. For motif presence analysis, we added all the motifs in the three groups. The cumulative occurrence of each motif at each time point was calculated and divided by the number of m^6A peaks per group. Then, each row of the final table obtained was reduced and centered to perform clustering of motif presence with in-house R scripts.

1.15 Peak annotation

The position of the peak around the transcript start sites of genes can predict the interaction sites of proteins and genes. PeakAnnotator (Salmon-Divon et al., 2010) was used to identify the nearest TSS of every peak, and the distance distribution between peaks and the TSS is shown. In addition, the distribution of peak on different functional regions, such as the 5'UTR, CDS, and 3'UTR, was determined.

GRCm38.p6 Ensembl 94 (ftp://ftp.ensembl.org/pub/release-94/fasta/mus_musculus/dna/Mus_musculus.GRCm38.dna.primary_assembly.fa.gz) was used for gene annotation. Peak-related genes were confirmed by PeakAnnotator, and then Gene Ontology (GO) enrichment analysis was performed to identify the functional enrichment results. GO enrichment analysis was implemented by the GOseq R package, in which gene length bias was corrected. GO terms with corrected *P* values less than 0.05 were considered significantly enriched by peak-related genes.

KEGG is a database resource for understanding the high-level functions and utilities of biological systems, such as cells, organisms and ecosystems, from molecular-level information, especially large-scale molecular datasets generated by genome sequencing and other high-

throughput experimental technologies (http://www.genome.jp/kegg/). We used KOBAS software to test the statistical enrichment of peak-related genes in KEGG pathways.

1.16 Peak analysis

The quantity statistics of peaks was according to the number of common (or summational, or merge) peaks in every three replicates of each group. Differential peak analysis was based on the fold enrichment or RPM of peaks of different experiments. A peak was determined as a differential peak when the odds ratio between two groups was greater than 2. Using the same method, genes associated with differential peaks were identified and subjected to GO and KEGG enrichment analyses.

1.17 MeRIP-qPCR

MeRIP assay was performed using Magna MeRIP m^6A Kit (Millipore, MA) following the manufacturer's instructions. Briefly, 200 μg of total RNA was extracted from bone marrow cells of mice. The fragmentation of RNA was conducted using RNase MiniElute Kit. Chemically fragmented RNA (~200 nucleotides) was incubated with m^6A antibody (Millipore) or mouse IgG-conjugated beads in 500 μL 1×IP buffer supplemented with RNase inhibitors at 4℃ overnight. Methylated RNA was immunoprecipitated with beads, eluted by competition with free m^6A, and recovered with RNeasy kit (Qiagen). One tenth of fragments of RNA samples were retained and labeled as input. Enrichment of m^6A containing mRNA in each sample was then analyzed by RT-qPCR and calculated by normalizing to ten-fold input. The primer sequences are listed in Supplementary Table S1.

1.18 Interfering with the expression of m^6A effector enzymes in vivo with siRNAs

Before irradiation began, the animal-applicable siRNAs targeting *METTL3*, *FTO* or

ALKBH5 were dissolved in normal saline (5 nmol in 200 μL) and immediately injected into the mouse tail vein (5 nmol/20 g). An equivalent volume of normal saline containing dissolved scrambled siRNA was injected as a control. The siRNA duplexes and their respective negative controls were synthesized and purified by RiboBio (Guangzhou, China), and the injection was repeated once after three days. For the 4 Gy irradiated group, mice were housed for 15 days and then sacrificed to collect blood, spleen and thymus; for the 7.2 Gy γ-irradiation group, mice were housed for 4 weeks to observe survival.

1.19 Fluorescence-activated cell sorting (FACS)

For hematopoietic progenitor cell (HPC, Lineage$^-$Scal$^-$c-kit$^+$) and hematopoietic stem cell (HSC, Lineage$^-$Scal$^+$c-kit$^+$) analyses (Li et al., 2009; Shao et al., 2014), bone marrow cells were isolated as previously reported (Li et al., 2009; Shao et al., 2014) (Zhang et al., 2016). Briefly, 5×10^6 cells were incubated with Biotin-conjugated antibodies specific for Gr1, Ter119, CD11b, B220, CD4, and CD8 (mixed Lineage antibodies) for 1 hour, and then stained with PerCP streptavidin, PE sca1, APC c-kit, and FITC CD34 antibodies for 30 min. Data acquisition was performed on a BD Accuri C6 flow cytometer and analyzed by the BD Accuri C6 software (BD Bioscience, San Jose, CA, USA).

References

Bailey, T.L. (2011). DREME: motif discovery in transcription factor ChIP-seq data. Bioinformatics 27, 1653-1659.

Bailey, T.L., Boden, M., Buske, F.A., Frith, M., Grant, C.E., Clementi, L., Ren, J., Li, W.W., and Noble, W.S. (2009). MEME SUITE: tools for motif discovery and searching. Nucleic acids research 37, W202-208.

Bailey, T.L., Johnson, J., Grant, C.E., and Noble, W.S. (2015). The MEME Suite. Nucleic acids

research 43, W39-49.

Gong, Y., Li, S.J., Liu, R., Zhan, J.F., Tan, C., Fang, Y.F., Chen, Y., and Yu, B. (2019). Inhibition of YAP with siRNA prevents cartilage degradation and ameliorates osteoarthritis development. Journal of molecular medicine 97, 103-114.

Gupta, S., Stamatoyannopoulos, J.A., Bailey, T.L., and Noble, W.S. (2007). Quantifying similarity between motifs. Genome biology 8, R24.

Krutzfeldt, J., Rajewsky, N., Braich, R., Rajeev, K.G., Tuschl, T., Manoharan, M., and Stoffel, M. (2005). Silencing of microRNAs in vivo with 'antagomirs'. Nature 438, 685-689.

Li, H., Xie, H., Liu, W., Hu, R., Huang, B., Tan, Y.F., Xu, K., Sheng, Z.F., Zhou, H.D., Wu, X.P., et al. (2009). A novel microRNA targeting HDAC5 regulates osteoblast differentiation in mice and contributes to primary osteoporosis in humans. The Journal of clinical investigation 119, 3666-3677.

Luo, Z., Zhang, Z., Tai, L., Zhang, L., Sun, Z., and Zhou, L. (2019). Comprehensive analysis of differences of N(6)-methyladenosine RNA methylomes between high-fat-fed and normal mouse livers. Epigenomics 11, 1267-1282.

Machanick, P., and Bailey, T.L. (2011). MEME-ChIP: motif analysis of large DNA datasets. Bioinformatics 27, 1696-1697.

Meyer, K.D., Saletore, Y., Zumbo, P., Elemento, O., Mason, C.E., and Jaffrey, S.R. (2012). Comprehensive analysis of mRNA methylation reveals enrichment in 3' UTRs and near stop codons. Cell 149, 1635-1646.

Salmon-Divon, M., Dvinge, H., Tammoja, K., and Bertone, P. (2010). PeakAnalyzer: genome-wide annotation of chromatin binding and modification loci. BMC bioinformatics 11, 415.

Shao, L., Luo, Y., and Zhou, D. (2014). Hematopoietic stem cell injury induced by ionizing radiation. Antioxidants & redox signaling 20, 1447-1462.

Wang, J., Wang, Y., Zhang, H., Chang, J., Lu, M., Gao, W., Liu, W., Li, Y., Yin, L., Wang, X., et al. (2020). Identification of a novel microRNA-141-3p/Forkhead box C1/beta-catenin axis associated with rheumatoid arthritis synovial fibroblast function in vivo and in vitro. Theranostics 10, 5412-5434.

Zhang, J., Xue, X., Han, X., Yao, C., Lu, L., Li, D., Hou, Q., Miao, W., Meng, A., and Fan, S.

(2016). Vam3 ameliorates total body irradiation-induced hematopoietic system injury partly by regulating the expression of Nrf2-targeted genes. Free radical biology & medicine 101, 455-464.

Zhang, S., Gao, S., Zhao, M., Liu, Y., Bu, Y., Jiang, Q., Zhao, Q., Ye, L., and Zhang, X. (2017). Anti-HBV drugs suppress the growth of HBV-related hepatoma cells via down-regulation of hepatitis B virus X protein. Cancer letters 392, 94-104.